arXiv:astro-ph/0106393v1 21 Jun 2001

The Gas Content and Kinematics of Nearby Blue Compact Galaxies: Implications for Studies at Intermediate and High Redshift.

D.J. Pisano & Henry A. Kobulnicky[1]

Astronomy Dept., U. Wisconsin - Madison

475 N. Charter St., Madison, WI 53706

pisano@astro.wisc.edu, chip@astro.wisc.edu

Rafael Guzmán[1]

Dept. of Astronomy, University of Florida

P.O. Box 112055, Gainesville, FL 32611

guzman@astro.ufl.edu

Jesús Gallego

Departamento de Astrofísica, Universidad Complutense de Madrid

E-28040 Madrid, Spain

jgm@astrax.fis.ucm.es

Matthew A. Bershady

Astronomy Dept., U. Wisconsin - Madison

475 N. Charter St., Madison, WI 53706

mab@astro.wisc.edu

ABSTRACT

We present Arecibo 21 cm spectroscopy, Keck HIRES Hβ spectroscopy, and WIYN R-band imaging of 11 nearby blue compact galaxies with effective B-band surface brightness SBe =19.4-21.2 mag arcsec^{-2} and effective radii R_{eff} =0.6-1.9 kpc. This sample was selected to test the reliablility of mass estimates derived using optical emission linewidths, particularly for the blue compact star-forming galaxies observed at intermediate redshifts ($0.1 < z < 1$). In addition, we also measure the H I content and gas

[1]Hubble Fellow

depletion timescales for the nearby blue, compact galaxies in an attempt to infer the present nature and possible future evolution of their intermediate redshift analogs. We detected H I in 10 of 11 sample galaxies. They have H I masses of 0.3–4$\times10^9$ $M_\odot$, H I linewidths, W_{20}, of 133–249 $km\ s^{-1}$, dynamical masses of 0.5–5$\times10^{10}M_\odot$, gas depletion timescales, τ_{gas}, of 0.3–7 Gyr, H I mass fractions of 0.01–0.58, and mass-to-light ratios of 0.1–0.8. These values span the range of values typical of nearby H II galaxies, irregulars and spirals. Despite the restricted morphological selection, our sample of galaxies is quite heterogeneous in terms of H I content, dynamical mass, and gas depletion timescale. Therefore, these galaxies have a variety of evolutionary paths and should look very different from each other in 5 Gyr. Those with high masses and gas depletion timescales are likely to retain their ISM for future star formation while the lower mass objects with small gas depletion timescales may be undergoing their last major event of star-formation. Hence, the fading of intermediate-redshift luminous blue compact galaxies into NGC205-type spheroidals is a viable evolutionary scenario, but only for the least massive, most gas-poor objects in this sample.

The most consistent characteristic of our morphologically-selected sample is that the ratios of H II linewidths to H I 21 cm linewidths, $\mathcal{R}=\frac{W_{20}(\mathrm{H\ II})}{W_{20}(\mathrm{H\ I})}$, are systematically less than unity, with an average value of $\mathcal{R}=0.66\pm0.16$; similar to findings for local H II galaxies. The simplest explanation for this result is that the ionized gas is more centrally concentrated than the neutral gas within the gravitational potential. We find that $\mathcal{R}$ is a function of linewidth, such that smaller linewidth galaxies have smaller values of $\mathcal{R}$. Correcting optical linewidths by this factor not only raises the derived masses of these galaxies, but also makes them consistent with the local luminosity–linewidth (Tully-Fisher) relation as well. If this ratio applies to intermediate-redshift galaxies, then the masses of intermediate redshift blue compact galaxies can be obtained from optical linewidths after applying a small correction factor, and the proposed luminosity evolution of the Tully-Fisher relation is much smaller and more gradual than suggested by studies using optical emission line width measurements.

1. Introduction

The Hubble Space Telescope and the new generation of 8 m class telescopes have extended our knowledge of the early Universe by identifying galaxies down to magnitudes B$\sim$28 and redshifts z$\geq$3 (see review by Ellis 1997). A current challenge is to understand the evolutionary connection between distant galaxies and their nearby counterparts. One approach is to compare fundamental galaxy parameters (i.e., sizes, masses, luminosities) of distant samples with better-studied nearby counterparts to help understand the harder-to-observe distant objects and establish evolutionary connections to present-day galaxies.

Studies of high redshift galaxies have revealed a population of compact, luminous galaxies

with high star formation rates (e.g., Steidel, *et al.* 1996a; 1996b, Lowenthal *et al.* 1997). At intermediate redshifts, apparently similar sources have been called by various names, including "Compact Narrow Emission Line Galaxies" (CNELG; Koo et al. 1994; 1995; Guzmán et al. 1996, 1998), "Blue Nucleated Galaxies" (BNG; Schade et al. 1995), and faint, compact galaxies (Guzmán et al. 1997; Phillips et al. 1997) depending on what properties are being emphasized, and how the samples were selected. It is worth noting that the term "Narrow" in the context of CNELG is with respect to QSOs and AGN; the CNELGs themselves display a range of kinematic emission line-widths between 30 and 130 $km\ s^{-1}$.

Jangren et al. (2001) have compared several of the brighter of the above intermediate-redshift samples. They find that while the sources display a range of photometric properties, most of the galaxies can be isolated quantitatively on the basis of their colors and image structure parameters as a class distinct from normal Hubble-types found in bright samples. They define one such class as "Luminous Blue Compact Galaxies" (LBCGs). Sources in this class have small sizes, high luminosities (hence high surface-brightness), and very blue colors. Their image concentration and asymmetry is slightly higher than for nearby irregular galaxies included in bright samples. However, this class of galaxies is not defined by their emission-line kinematic widths.

The nature and evolution of the LBCG class at intermediate redshift are currently major issues under debate. The most comprehensive studies of the LBCG population at intermediate redshift to date are those of Phillips et al. (1997) and Guzmán et al. (1997). They concluded that the LBCG class is populated by a mixture of starburst galaxies. About 60% of galaxies in their sample are classified as "HII-like" since they are similar to today's population of luminous, young, star-forming HII galaxies. The remaining ∼40% are classified as "SB disk-like" since they form a more heterogeneous class of evolved starbursts similar to local starburst spiral and irregular galaxies. This classification is consistent with the results published for other LBCG samples in the literature. For instance, Koo et al. (1994, 1995) and Guzmán et al. (1996, 1998) first established the association between HII galaxies and LBCGs for their sample of CNELGs. Alternatively, Mallén-Ornelas et al. (1999) and Hammer et al. (2000), have concluded that their LBCG samples can be best identified with bright irregulars, late-type spirals or even more massive spirals with a very young bulge.

Given the diverse nature of the LBCG population, it is most likely that they will not evolve into one homogeneous galaxy class. Rather, different LBCGs may evolve into different galaxy classes. There are two main evolutionary scenarios currently discussed in the literature. Koo et al. (1994) and subsequent authors have suggested that some subset of the most compact HII-type LBCGs at intermediate redshifts may be the progenitors of local low-mass elliptical galaxies (also called spheroidals), such as NGC 205. Their conjecture is based on the similarity of the kinematic widths and sizes of the LBCGs with low-mass ellipticals. Evolutionary models predict that, in 4-6 Gyr of passive evolution, the faded luminosities and surface brightnesses of HII-type LBCGs will match local low-mass ellipticals. This evolutionary prediction requires that LBCGs are undergoing their last major burst of star formation at a z∼0.4. In order to match the low luminosities of

low-mass elliptical galaxies, star formation in HII-type LBCGs must be short-lived (timescales $\sim$ 1 Gyr or less) so that they fade by $\sim$2-4 magnitudes in $\sim$4-6 Gyr (Guzmán *et al.* 1998). Since local low-mass ellipticals have little detectable cool gas (Young & Lo 1997; Young 2000), this prediction also requires HII-type LBCGs to lose nearly all of their gas by the present day. Alternatively, the evolutionary scenario for SB disk-like LBCGs currently being considered is very different. Some authors have suggested that these LBCGs may actually be disks forming from the center outward to become present-day spirals (Phillips et al. 1997; Hammer et al. 2000). Thus SB disk-like LBCGs would be more massive than inferred from their virial masses since their small sizes and kinematic emission-line widths would reflect mainly the central starburst region (Phillips et al. 1997; Barton & Van Zee 2001). These objects are also expected to have large reservoirs of gas that may allow for continuing star formation, albeit at a lower rate than the current burst.

Measurements of the 21 cm neutral hydrogen (H I) linewidth and flux may provide an important new constraint on the evolution of LBCGs. The H I linewidth is a very good indicator of the rotational velocity of a galaxy, provided the system is not severely distorted or interacting. We can use this rotational velocity to obtain a total enclosed mass of the system, a parameter that will not change dramatically with time (at least over the past few gigayears), unlike the star formation rate or luminosity. H I measurements typically trace gas out to a larger radius than the optical emission lines and, hence, offer a more robust measurement of the mass. An integrated HI line flux, coupled with an adopted distance, provides a measure of the total neutral hydrogen mass which limits a galaxy's potential for future star formation. The H I mass and a known star formation rate (SFR) help set limits on the timescale for the reservoir of neutral gas to be depleted.

Since neutral hydrogen observations of the intermediate redshift LBCGs are not yet possible, we must infer their properties from nearby analogs. This is possible provided the nearby sample is representative of the more distant LBCGs. If observations imply that one of our analogs has a small H I linewidth, a small quantity of neutral gas, and a short gas depletion timescale, then the case is strengthened for it being a low-mass object which will shortly cease star formation and undergo subsequent passive evolution. If, on the other hand, observations imply a large H I linewidth, a large reservoir of neutral gas, and a long gas depletion timescale, then the analog would appear to be a higher-mass galaxy. A long period of passive evolution following the end of the current starburst would seem less likely and the galaxy may continue having subsequent events of star formation.

Because we wish to consider sources which span a range of luminosities from "dwarf" ($M_B > -18$) to "luminous" ($M_B < -18$), we adopt here the more generic term Blue Compact Galaxy (BCG) to encompass this diverse group of small, blue galaxies regardless of luminosity or kinematics. Throughout this paper, we will use the sample of compact galaxies in the Hubble Deep Field flanking fields (HDF-ff; Guzmán et al. 1997; Phillips et al. 1997), intermediate redshift CNELGs (Koo et al. 1994, 1995; Guzmán et al. 1996), and the BNGs of Schade et al. (1995) as a benchmark for assessing a population of local compact galaxies. We will refer to these previous samples collectively as the intermediate-redshift BCGs.

Another issue relating to the study of intermediate redshift galaxies that we will examine concerns the Tully-Fisher (T-F) relation and its evolution. Specifically, studies of the internal kinematics of intermediate redshift galaxies have led to discrepant results on the evolution of the T-F zeropoint. For example, Forbes et al. (1996), Rix et al. (1997), Simard & Pritchet (1998), and Mallén-Ornelas et al. (1999) all find between 1 and 2 magnitudes of brightening in the T-F at redshifts of 0.2-0.8. These surveys rely on [OII] or [OIII] & Hβ emission-lines as kinematic tracers; all except Simard & Pritchet measure spatially integrated line-widths. In contrast, studies using resolved rotation curves at intermediate redshifts (Vogt et al. 1996, 1997; Bershady et al. 1999) find much less brightening (0-0.6 mag) over a range of redshift between 0.1 to 1. Many of these studies specifically target blue galaxies, some of which undoubtedly are BCGs by virtue of their strong emission lines and high surface-brightness.

One question that has arisen is whether the spatially-integrated line-widths of optical emission lines used in some studies under-estimate the true rotation velocities. Indeed, Forbes et al. (1996) note that in two cases where they have resolved rotation curves, their line-widths under-estimate the true rotation speed by 2% and 41%, respectively. Complicating the issue is the fact that the different studies select heterogeneously from the distant galaxy population (Bershady 1997). If different galaxies evolve at different rates, the measured evolution in the T-F zeropoint may depend on galaxy types sampled, as suggested by Simard & Pritchet (1998). They find tentative evidence that the least-massive (slowest rotators) brighten most. While they have measured rotation-curves (albeit at limited spatial resolution and low S/N), the sense of this observation is the same as would result from the systematic under-estimate of true line-width based on optical measurements. We are in a position here to address the reliability of internal kinematics based on spatially-integrated, optical emission line-widths, as well as the conclusions drawn from these measurements.

In this paper we are presenting H I and H II spectroscopy, as well as R-band imaging, of 11 nearby BCGs drawn from the Universidad Complutense de Madrid (UCM) emission-line survey (Zamorano *et al.* 1994). These galaxies were selected to morphologically resemble the BCG population at intermediate redshift. In section 2 we present the sample selection criteria, observing procedure, and reductions. Section 3 contains the analysis of the data. In section 4 we present our sample galaxies. We discuss the implications of our observations for the inherent nature of BCGs in section 5, and we conclude in section 6. We adopt $H_0 = 70\ km\ s^{-1}\ Mpc^{-1}$ and $q_0 = 0.05$ throughout this paper.

2. Data & Observations

2.1. Sample Selection

Most BCGs at intermediate redshifts ($z \sim 0.4$) that have been discussed in the literature are intrinsically luminous objects ($M_B < -18$ mag), with blue rest-frame colors ($B - V < 0.45, B -$

$r < 0.6$), and compact in the sense that they have high effective B-band surface brightnesses[2] ($SB_e < 21.5$ mag arcsec^{-2}). For this study, we chose galaxies which would be nearby analogs to intermediate-z BCGs. Sample galaxies were chosen from the UCM emission line survey of star forming galaxies (Zamorano *et al.* 1994; 1996) based on data from the original survey, follow-up optical spectroscopy (Gallego *et al.* 1996; 1997) and optical photometry (Vitores *et al.* 1996a; 1996b; Pérez-González *et al.* 2000). The survey preferentially selects objects with large Hα emission line equivalent widths, $EW > 50$Å. Four physical parameters were used to identify the nearby counterparts to the objects observed at intermediate redshift: luminosity, color, velocity dispersion (σ) of the optical emission lines, and effective radius. The criteria were chosen to exclude very low luminosity systems and Blue Compact Dwarfs, in the classical sense ($M_B \geq$ -17.0), to include objects with blue color, $B-r \leq 1.0$, and those with small sizes, $R_{eff} \leq 2.0$ kpc, and small velocity dispersions, $\sigma_{\rm H\ II} < 80\ km\ s^{-1}$. The important constraint is that our sample galaxies have visible properties similar to BCGs at higher redshifts. We further restricted the sample to objects with declinations between -1° and +38° in order that they be observable from Arecibo. From this limited sample we chose 11 galaxies, which tended to have the smallest velocity dispersions. Table 1 lists the targets selected for observation, their positions, and the time-on-source, along with alternate identifiers and comments.

In Figure 1 we compare the luminosity, color, size, and surface brightness of the 11 UCM sample galaxies (filled circles) with intermediate redshift BCGs from the Hubble Deep Field flanking fields (open triangles; denoted HDF-ff; Phillips et al. 1997; Guzmán et al. 1997) and with a sample of BCGs (open boxes, including the Compact Narrow Emission Line Galaxies of Koo et al. 1994, 1995 and the Blue Nucleated Galaxies of Schade et al. (1995)). The polygons (from Phillips *et al.* 1997, figure 8) illustrate the approximate location of nearby elliptical, spiral, irregular, and spheroidal galaxies. Figure 1 demonstrates that our sample galaxies have similar surface brightnesses, absolute magnitudes, and colors to the intermediate redshift BCGs from the literature. In addition, our galaxies have surface brightnesses more similar to low-mass ellipticals and high-mass spheroidals than to massive spirals or irregulars. Some of the targets are on the border between these two classes of objects. While our galaxies do not occupy the full range of parameter space that the intermediate redshift BCGs do, they are sampling a significant subset of the BCG properties. Our galaxies cover almost the full range of luminosities and colors as the intermediate-z BCGs, but are only comparable to the smallest of the distant BCGs (with $SB_e \sim$20 mag arcsec^{-2}). These limitations must be remembered when we compare our sample galaxies with their more distant counterparts.

[2] $SB_e = 5 \times log[R_{eff}(kpc)] + M_B + 38.6$. This is the average surface brightness inside the half-light radius, equivalent to the effective radius for a $r^{1/4}$ profile.

2.2. H I Observations

HI observations of the 11 sample galaxies were made using the Arecibo[3] 305 m telescope on 1999 October 14-16. We observed from 2200-0400 LST each day using the 1.4 GHz feed in conjunction with the L-narrow and L-wide receivers. The L-wide receiver was only used for observations of UCM 0135+2242, while the L-narrow receiver was used for the remaining 10 galaxies. This configuration has a beamwidth of $3.'4 \times 3.'8$ (79×88 kpc for a typical galaxy distance of 80 Mpc) and a measured gain of 10 K Jy^{-1}. The system temperature has been measured at 32 K for the L-narrow receiver and 38 K for the L-wide receiver. We observed in 4 IFs, recording data in two separate bandwidths in both polarizations simultaneously. We observed with bandwidths of 12.5 MHz and 25 MHz with 9-level sampling. This yields a velocity coverage of $\sim$2500 $km\ s^{-1}$and $\sim$5000 $km\ s^{-1}$, respectively. With 2048 channels for each IF, the velocity resolution is 1.3 $km\ s^{-1}$ and 2.6 $km\ s^{-1}$, respectively. Because the different subcorrelators are not fully independent, we could not combine the two separate bandwidths to improve the sensitivity of our observations.

The observing procedure involved looking at the galaxy for 6 minutes and then doing an off-source scan over the same zenith angle and azimuth range for an additional 6 minutes. We repeated observing these on-off pairs until we felt we had a firm detection, or that no detection was easily forthcoming. Time on source and measured noise levels for each target are presented in Tables 1 & 2 respectively.

2.3. H I Reductions

Calibration of the data was done using the Arecibo package, ANALYZ. We started by combining each pair of on-off scans by taking $\frac{on-off}{off}$. Each combined pair was then corrected for gain and T_{sys} variations with zenith angle and converted from T_B in Kelvins to flux in Janskys using the tabulated gain factors from the Arecibo Users' Manual. This factor is roughly 3.6 Jy K^{-1}, but varies with the zenith angle of the observation. All scans for a given galaxy were then averaged together. We then averaged the two polarizations for each galaxy together to get a combined un-polarized spectrum. Finally, we did a first or second order baseline subtraction on the unpolarized, combined spectrum to get our final, calibrated, reduced spectrum of flux versus heliocentric velocity. As a check on our reductions, we compared the total H I flux with previously published values for UCM 2325+2318, otherwise known as NGC 7673. We find that the H I flux agrees to within 5% of the value found by Nordgren *et al.* (1997a) with the VLA. The data was then ported into IDL for the analysis. Figure 2 shows the calibrated H I spectra for all observed galaxies as the light grey lines.

[3]The Arecibo Observatory is part of the National Astronomy and Ionosphere Center which is operated by Cornell University under a Cooperative Agreement with the National Science Foundation.

2.4. Keck Echelle Spectroscopy & Reductions

At the Keck I 10 m telescope[4] we used the HIRES spectrograph (Vogt *et al.* 1994) with the blue cross disperser to obtain R ∼30,000 spectra over the wavelength range 3600 - 5200 Å. Observing occurred 1999 October 14-15 and 2000 September 14-15. The primary goal was to use the Hβ λ4861 emission line to measure the kinematics of the ionized gas. For two galaxies, UCM 2351+2321 and UCM 2325+2318, the redshifted Hβ line fell at the edge of the detector, so we instead use the [O III] λ4959 line in the following analysis. The slit decker D1 measuring 1.15″ in the spectral direction and 14.0″ in the spatial direction was used for all objects except UCM0135+2242, UCM0148+2123, and UCM0159+2354 where the C5 slit decker measuring 1.15″×7.0″ was used. Periodic exposures of a Th-Ar arc lamp were used to establish the radial velocity and dispersion. The wavelength zeropoint of each exposure is good to an RMS of 0.003 Å. The mean instrumental resolution was 0.12 Å FWHM (7.4 $km\ s^{-1}$) at 4900 Å based on exposures of arc lamps. One 1200 s exposure was obtained for each object. During each exposure, the telescope was moved in order to drift the slit slowly across each target to simulate a "spatially integrated" spectrum that would be obtained if all objects were unresolved at large distances. Inspection of the resulting spectra showed that the 14″ slit was long enough to cover the entire emission line region of each galaxy, except in the case of UCM2325+2318 where portions of the low-surface brightness disk extended beyond the ends of the slit. In the reduction process, each spectrum was summed along the spatial dimension to produce a 1D emission line spectrum. The resulting optical emission line spectrum for each galaxy is shown overplotted in black on the H I spectrum in Figure 2. There is good correspondence between the H I and H II systemic velocities, confirming that we have correctly identified objects placed at the center of the Arecibo beam. W_{20} has been calculated from the H II line for each galaxy observed and the results appear in Table 2. A comparison of our spatially integrated spectra with the single position spectra of Gallego et al. (2001, in preparation) show that our values are larger, on average, by 7% with an RMS deviation of 19%. Therefore the linewidths of our galaxies are statistically the same regardless of whether they are measured at a single position or are spatially-integrated.

2.5. WIYN Imaging

We obtained R-band images of all 11 galaxies with the WIYN[5] 3.5 m telescope using the Mini-Mosaic 4k×4k CCD camera during 2000 October 16-17 and November 17-18 in 1.2″ (mean) seeing. The pixel scale was 0.141 arcsec/pixel, and integration times were 1-2 ×300 s. The images were

[4]Some of the data presented herein were obtained at the W.M. Keck Observatory, which is operated as a scientific partnership among the California Institute of Technology, the University of California and the National Aeronautics and Space Administration. The Observatory was made possible by the generous financial support of the W.M. Keck Foundation.

[5]The WIYN Observatory is a joint facility of the University of Wisconsin-Madison, Indiana University, Yale University, and the National Optical Astronomy Observatories.

reduced in the standard manner. We use these images below to characterize the morphology of each galaxy and supplement the data available in the literature (e.g., Vitores et al. 1997; Gallego et al. 1996). Rotational asymmetries, A, were computed following the procedures and method specified in Conselice et al. (2000); half-light radii, R_{eff}, and concentration indices, C, were computed following the procedures specified by Bershady et al. (2000). These values are therefore on the same system as computed for the Frei (1999) local galaxy sample by these authors.

Because the half-light radii were in the range of 1.5 to 9 arcsec, there were cases when we needed to apply corrections to the asymmetry values, half-light sizes, and concentration indices to account for the seeing. The corrections are in the sense of increasing the asymmetry and image concentration, while decreasing the half-light radius. The corrections for asymmetry are based on the simulations presented in Figure 19 of Conselice et al. (2000), and generally resulted in changes $< 15\%$. However, we note that the simulations included only one source plausibly similar to these sources: NGC 4449. To correct the half-light sizes and concentration indices, we modeled the effects of seeing based on a simulated grid of aberrated, two-dimensional analytic light distributions ($r^{1/4}$-law and exponential profiles with a range of axial ratios). The corrections to the half-light radii were generally under 15% and the changes in the concentration indices were typically a few tenths in the index. A comparison of our half-light radii and concentration indices with previous determinations show agreement of the means to 1% and 28% with an RMS deviation of 21% and 12%, respectively, to Vitores et al. (1996) and 6% and 1% for the mean with RMS deviation of 21% 17% to Peŕez-González et al. (2000), with few outliers. Our adopted WIYN values for R_{eff}, C, and A are listed in Table 3. For all subsequent discussions we will use these values, as determined from the WIYN images.

3. Analysis

For each galaxy we measured the total H I flux, the 20% velocity width, and the central velocity of each galaxy as listed in Table 2. The total H I flux was determined by integrating under the spectrum from where the galaxy first appears from the noise, to where it becomes indistinguishable from the noise. The RMS was measured from the off-line region and used to determine the error on the integrated flux. For UCM 2351+2321, which was not detected, the 3σ upper limit to the flux is set for an assumed H I velocity width equal to the optical width as noted in Table 2. The optical velocity widths come from our Keck observations. As most of the galaxy spectra rise very slowly out of the noise, we Hanning smoothed the spectra to assist in determining the 20% velocity width. Typically, we Hanning smoothed over 3 or 5 channels, then we used a program to identify all crossings of the 20% of peak intensity. We selected the most probable velocity width from these options. The cited velocity center is simply the midpoint between the 20% crossings. The errors on these values represent the approximate range of widths (and central velocities) due to the uncertainty determining the 20% crossing points. For UCM 2351+2321 the optical recession velocity is cited, and used to calculate a distance, due to the lack of a detection in H I. This

distance is listed in Table 3 and is used to calculate distance-dependent quantities such as H I mass, luminosity, and linear size.

We have also attempted to derive the dynamical masses for these galaxies. To do this we need a rotation velocity and a radius corresponding to that velocity. We used half of the inclination-corrected W_{20} as a reasonable approximation for the rotation velocity. For the corresponding radius, $R_{H\ I}$, we scaled the effective radius, R_{eff}, determined from our WIYN images, up by a factor of 4.5. This factor is based on the ratio of the R_{eff} to $R_{24.5}$ found for these galaxies in Vitores *et al.* (1996), which was 2.4. We rounded this up to 2.5 to get an estimate of R_{25}, and then multiplied R_{25} by 1.8 to get $R_{H\ I}$, based on the observed ratio of R_{25} to $R_{H\ I}$ found by Broeils (1992) for nearby gas-rich galaxies. $R_{H\ I}$ may even be higher as van Zee, Skillman, & Salzer (1998) find $R_{H\ I}/R_{25}$ ranging from 2.8-4.9 for a sample of 5 H II galaxies. Using $R_{H\ I}$ and V_{rot}, we calculate an estimate for the dynamical mass:

$$M_{dyn} = \frac{V_{rot}^2 R_{H\ I}}{G}. \quad (1)$$

Table 4 lists these dynamical masses along with the hydrogen gas mass fraction, $f_{gas}=M_{H\ I}/M_{dyn}$. Tables 3 and 4 also list the optical properties of the sample galaxies, including absolute blue magnitudes, M_B, B-r and B-V colors computed within the 24 mag arcsec^{-2} isophote, the effective surface brightness within the 24 mag arcsec^{-2} isophote, the Hα luminosity, and the inclination of these galaxies (from Vitores et al. 1996a, 1996b; Gallego et al. 1996, 1997; Peŕez-González et al. 2000).

To assist in examining the evolutionary potential of these galaxies we calculated the star formation rates for these galaxies from the listed redenning-corrected Hα luminosities (Gallego *et al* 1996) using the expression given in Kennicutt (1983):

$$SFR(M_\odot\ yr^{-1}) = \frac{L_{H\alpha}}{1.12 \times 10^{41}\ erg\ s^{-1}} \quad (2)$$

Using the star formation rate and the H I mass of each galaxy, we calculate the gas depletion timescale, $\tau_{gas} = M_{HI}/SFR$ listed in Table 4. These estimates do not account for recycling of the gas, for the presence of helium ($\sim 40\%$ of the H I mass), or for molecular gas. All of these factors would increase τ_{gas}[6]. It is important to note that the $L_{H\alpha}$ values from Gallego et al. (1996) were measured through the spectrograph slit. Therefore they only represent a fraction of the total $L_{H\alpha}$ of the galaxy as would be measured via narrow-band imaging. Correcting for this underestimate would decrease our estimates of τ_{gas}. It is unclear, however, how to determine the extent of this correction with our current data.

[6]If we use the updated expression from Kennicutt *et al.* (1994) the SFR will be lower by $\sim$10% (τ_{gas} will be higher by the same amount). The expression from Alonso-Herrero *et al.* (1996) will decrease the SFR and increase τ_{gas} by a factor of 2.8.

Images of the target galaxies appear in Figure 3 and 4. Figure 3 shows Digital Sky Survey (DSS) images centered on the observed target coordinates. Each image is 3.′8 on a side, to match the angular size of Arecibo beam and assist in determining the nature of the objects we observed. Figure 4 shows the WIYN R-band images of our sample galaxies using a logarithmic greyscale. In order to facilitate comparison between galaxies, we have scaled these images so that each dimension covers a projected distance of 10 kpc at the adopted distances listed in Table 3.

4. Galaxy Properties

4.1. UCM 0014+1829

Optically, UCM0014+1829 has an oblong central region with a more diffuse outer disk. There is a bright star very close to the nucleus which complicates the determination of its optical properties. No other galaxies are evident in the DSS image. UCM 0014+1829 has the second largest half-light radius, 1.7 kpc, in our sample, and is one of the more concentrated objects as well, C=4.08. It is relatively symmetric, A=0.08. The H I profile is single peaked and slightly asymmetric. The H II spectrum is symmetric, centered at the same velocity as the peak of the H I profile, but is narrower with a width of 117 $km\ s^{-1}$ vs 204 $km\ s^{-1}$. A low amplitude wing to low velocity is evident in both spectra.

4.2. UCM 0040+0220

UCM 0040+0220 is the featureless point source in the middle of the DSS image. It has a small size (R_{eff}=0.6 kpc), is symmetric (A=0.09), and is not very concentrated (C=3.0). This galaxy has one of the smallest τ_{gas} values, 0.41 Gyr, of our sample due, in part, to its low $M_{H\ I}$, $2.6\times10^8 M_\odot$. While there is a strong double-horned H I profile at ∼4500 $km\ s^{-1}$, UCM 0040+0220 is the weaker feature at ∼5400 $km\ s^{-1}$. The other features at higher recession velocities may be real, but we do not have the signal-to-noise ratio in this observation to confirm them. The H I profile is somewhat asymmetric, but is hard to characterize due to its low signal-to-noise ratio. The H II spectrum has a tail to lower velocity, similar to that in the H I profile. The double-horned H I profile at ∼4500 $km\ s^{-1}$ is most likely the diffuse galaxy east of UCM 0040+0220 in the DSS image.

4.3. UCM 0056+0043

Our WIYN image of UCM 0056+0043 reveals that it is slightly extended in the east-west direction. No other galaxies are evident in the DSS image of the field. This galaxy has a half-light radius of 0.9 kpc, an average concentration of 2.96, and a low asymmetry of 0.07. The H I spectrum of UCM 0056+0043 is a strong single peak with weak high velocity wings extending to

lower redshift. The profile is slightly asymmetric. The H II spectrum matches the H I profile very closely, with an absence of high-velocity wings. The H II width (126 $km\ s^{-1}$) is nearly identical to the H I width (133 km s^{-1}). This galaxy has the smallest width of all our sample galaxies, the smallest dynamical mass ($5\times10^9 M_\odot$), and the highest gas mass fraction at 0.58. It also has one of the longest gas depletion timescales, 6.3 Gyr.

4.4. UCM 0135+2242

This galaxy has a rather extended, diffuse disk evident in its WIYN image with a large R_{eff}=1.4 kpc. The concentration is high at 4.0, and the galaxy is very symmetric, A=0.02. UCM 0135+2242 is one of the most massive galaxies in our sample, $M_{dyn}=4.4\times10^{10} M_\odot$, and has a long τ_{gas} of 2.5 Gyr, despite its high SFR of 1.7 $M_\odot\ yr^{-1}$. A potential small companion is evident just to the southwest in the image as well. The DSS image reveals another diffuse galaxy at the southern most extent of the Arecibo field, which may or may not be associated. UCM 0135+2242 has a double-horned H I profile which is slightly asymmetric. The H II profile is narrower (W_{20}=225 $km\ s^{-1}$) and more symmetric than the H I profile (W_{20}=249 $km\ s^{-1}$). Intriguingly, the low redshift peak of the H I profile is broader and stronger than the H II peak. In other words, the peak of the H I distribution does not contain corresponding H II emission. This asymmetry in the H I profile, and discrepancy with the H II profile, may indicate that multiple galaxies were observed in the Arecibo beam, and/or that an interaction has occurred.

4.5. UCM 0148+2123

UCM 0148+2123 either has a double nucleus, or is two related objects which are possibly merging based on our WIYN image of the galaxy. No other galaxies are evident in the Arecibo beam. The morphological parameters suggest that this galaxy is not particularly large, R_{eff}=1.0 kpc, nor concentrated, C=2.72, but it is quite asymmetric, A=0.13. The latter point is not surprising given the double-lobed appearance of this galaxy. In addition, this galaxy has one of the smallest τ_{gas}, 0.65 Gyr, meaning it will rapidly use up its $3.8\times10^8 M_\odot$ of H I. This could be indicative of an ongoing interaction. UCM 0148+2123 has a asymmetric single-peaked H I profile, which may be caused by two galaxies being observed. As with most of our galaxies, the H II profile is narrower (W_{20}=98 $km\ s^{-1}$) and more symmetric than the H I profile (W_{20}=200 $km\ s^{-1}$). The H I profile extends further to lower velocities than the H II profile does, suggesting a difference in the neutral and ionized gas distributions

4.6. UCM 0159+2354

UCM 0159+2354 features an elongated core and extended, diffuse disk indicative of a highly inclined system. There may be some small, faint galaxies also in this field, but it is not at all clear if they are associated with our target galaxy. While UCM 0159+2354 has a normal R_{eff}, 1.0 kpc, it is the most concentrated galaxy in our sample, 4.25, and is also optically asymmetric, A=0.12. Also, UCM 0159+2354 is the reddest galaxy in our sample with a B-r color of 1.00. The H I spectrum shows a single-peaked profile for this galaxy. The center of the H II spectrum is offset in velocity from the H I profile (4925 $km\ s^{-1}$ vs. 4901 $km\ s^{-1}$). The H II profile is also narrower (138 $km\ s^{-1}$ vs. 192 $km\ s^{-1}$). This may indicate a real difference in the distributions of the neutral and ionized gas.

4.7. UCM 2251+2352

There are two galaxies apparent in the H I spectrum of UCM 2251+2352. While both detections have similar widths, the one at higher redshift is significantly brighter and is our desired target, based on its coincidence with the H II profile. The H I profile is wider than the H II profile (140 $km\ s^{-1}$ vs. 79 $km\ s^{-1}$), mostly due to high-velocity wings, while the central profiles match quite well. The Digitized Sky Survey image shows a few faint galaxies to the south and west of our target galaxy, but it is not clear if this is what we have detected at lower redshift in our H I spectrum. Our WIYN R-band image reveals a very faint, nearly face-on, barred spiral structure. The face-on nature of this galaxy makes any dynamical mass determination highly uncertain, due to the large inclination corrections needed. UCM 2251+2352 has a somewhat extended disk, with R_{eff}=1.4 kpc, and is relatively concentrated, C=3.43. It is, however, the most asymmetric galaxy in our sample, with A=0.27.

4.8. UCM 2304+1640

UCM 2304+1640 has a bright core, with a faint, extended, diffuse disk surrounding it. The DSS image of the field shows multiple diffuse objects, suggesting that we may have a spectrum of a galaxy group. The half-light radius of UCM 2304+1640 is one of the smallest in our sample at 0.7 kpc. The galaxy is rather concentrated, C=3.35, and asymmetric, A=0.12, as well. This galaxy has a single-peaked H I profile which is somewhat rounded on top; this would be consistent with observing a group of galaxies as seen in the DSS image. The H II profile is more symmetric, narrower, and slightly offset from the peak of the H I profile, also consistent with multiple objects being in the Arecibo beam.

4.9. UCM 2325+2318

Both the WIYN and DSS images of UCM 2325+2318, also known as NGC 7673, clearly shows signatures of interactions, with loops and a tail apparent around the main galaxy. This is the most extended galaxy in our sample, R_{eff}=1.9 kpc, and not very concentrated, C=2.98. UCM 2325+2318 is also the most asymmetric galaxy we observed, with A=0.60. Conselice, Bershady & Gallagher (2000) measured the same A value based on earlier WIYN imaging, and noted this galaxy has a large ratio of W_{20} to W_{50}. These authors found that a large value of this ratio was correlated with morphology, indicative of recent interactions. Consistent with this, Gallego *et al.* (1996) have identified three components in their H II spectrum of this galaxy and stated that this is an interacting system. Nordgren et al. (1997a) observed the H I disk of this system to be disturbed. NGC 7673 is also a well-known luminous FIR source (Sanders & Mirabel 1996); not surprising considering that the SFR is 23.5 $M_{\odot}\ yr^{-1}$, yielding τ_{gas}=0.18 Gyr. This is the highest SFR and shortest τ_{gas} in our sample. UCM 2325+2318 has a very strong, single-peaked H I profile. which has been studied in detail by Homeier & Gallagher (1999) with spectra from the WIYN DensePak integral field unit. In particular, they have measured the velocity field of this galaxy in the plane of the sky yielding a better estimate of its rotation velocity, W_{20}=126 $km\ s^{-1}$ vs. W_{20}=119 $km\ s^{-1}$ from our Keck spectrum; a fine agreement. The H II profile is narrower than the H I profile (W_{20}=119 $km\ s^{-1}$ vs. 164 $km\ s^{-1}$), and the relative positions of the peaks differ by $\sim 10\ km\ s^{-1}$.

4.10. UCM 2329+2512

The WIYN image of UCM 2329+2512 reveals a very small (R_{eff}=0.6 kpc), concentrated (C=4.15) galaxy with a faint, stellar loop, possibly indicative of a recent interaction. Despite this signature of interaction, it is remarkably symmetric, A=0.02. The low asymmetry is because the measurement of asymmetric is only in the central 7″, and is dominated by the bright central region, and not the faint loops. The faint loops could just be the projection of a strong two-armed spiral pattern in a highly inclined disk, and not a tidal tail. The symmetric, double-horned H I profile would support the idea that this system has not been disturbed. UCM 2329+2512 also has a low SFR, and the longest τ_{gas}, 7.3 Gyr, of our sample. No other galaxies are apparent in the DSS image of the Arecibo field. The H II spectrum of this galaxy is completely different from the H I profile, with a symmetric single-peaked profile. This suggests that the limited star formation in this galaxy is taking place only in the central regions, while the H I is much more extended.

4.11. UCM 2351+2321

We did not detect H I in UCM 2351+2321. The 3σ upper limit on its H I mass is 1.3×10^8 $M_{\odot}$ for an assumed width 160 $km\ s^{-1}$ (from the H II spectrum). There is a hint of H I emission near

where the H II profile rises at high velocity, but it is too weak to be a definite detection. Optically, UCM 2351+2321 is one of the reddest (B-r = 0.94 mag) and most concentrated, C=4.02, targets. In some respects, this is the most interesting galaxy of the entire sample because of the strong Hα emission, yet weak H I emission, implying a very small gas depletion timescale of <0.03 Gyr. If any galaxy among our sample represents a transition type between a gas-rich starburst and a gas-poor spheroidal, this may be such an object.

5. Discussion

5.1. Kinematics of Local Blue Compact Galaxies

The most interesting feature of our sample is that the ratio of H II to H I 21-cm linewidths, $\mathcal{R}$=W_{20}(H II)/W_{20}(H I), is always below unity. A further examination of the observed H II and H I profiles in Figure 2 shows that all but one of the H II spectra (UCM 0135+2242) and all but two of the H I spectra (UCM 0135+2242 and UCM 2329+2512) are single peaked, indicative of either extremely face-on disks or solid body rotation curves commonly seen in H II galaxies (e.g., van Zee et al. 1998). The latter option is more likely due to the large velocity widths of the lines, despite being singly-peaked.

Figure 5 plots $\mathcal{R}$ versus the H II emission linewidths, W_{20}(H II). Filled circles denote galaxies from this paper, while crosses denote the spiral and irregular galaxies studied by Kobulnicky & Gebhardt (2000), triangles denote the spiral sample of Raychaudhury et al. (1997), and squares are the H II galaxies from Telles & Terlevich (1993). It is evident from the figure that the H II–H I linewidth ratio systematically departs from unity for small H II linewidths. This effect is most prevalent for galaxies with W_{20}(H II)$\leq$ 200 $km\ s^{-1}$. The compact galaxies from our paper show a systematic difference between the neutral and ionized gas kinematics, such that they have a mean $\mathcal{R}$=0.66$\pm$0.16, which is different from most normal galaxies with a ratio closer to one. Our galaxies are similar, in this respect, to the H II galaxies and H II regions studied by Telles & Terlevich (1993) which have linewidth ratios $\sigma_{[O\ III]}/\sigma_{\rm H\ I}$ $\sim$0.7. Figure 5 illustrates that this discrepancy between the H II and H I linewidths seems to vary smoothly from large linewidths to small. Therefore, we have attempted to quantify this effect for all galaxies through an approximate polynomial fit to the data as follows:

$$\mathcal{R} = \frac{W_{\rm H\ II}}{W_{\rm H\ I}} = 1 - 5\ W_{\rm H\ II}^{-1} - 500\ W_{\rm H\ II}^{-2} - 2.5 \times 10^5\ W_{\rm H\ II}^{-3} \quad (3)$$

This equation yields a very rapid drop-off in $\mathcal{R}$ below W_{20}(H II) = 100 $km\ s^{-1}$, which becomes unphysical below W_{20}(H II) = 68 $km\ s^{-1}$. Since we have not observed $\mathcal{R}$ values below 0.4, we suggest that when applying the above formula, a lower bound of 0.3 is imposed.

Note that there is still a large scatter around this fit, so this formula should be applied with

great caution. A likely interpretation of the data is that the optical emission lines trace a smaller portion of the gravitational potential than the H I does, particularly in those galaxies with the smallest linewidth galaxies (i.e., σ <40 $km\ s^{-1}$). For these galaxies, the dynamical masses based on the width of optical emission lines will underestimate their masses by factors of 2-4. However, for galaxies with velocity widths σ larger than ∼40 $km\ s^{-1}$ the effect on the mass estimates is only <20%.

In addition to the observed dependence on velocity width, we have attempted to find a set of observational parameters which can identify galaxies in which the linewidth ratio, $\mathcal{R}$, is small. While we searched for correlations between all the observed parameters (color, SFR, concentration, asymmetry, R_{eff}, SB_e, etc.) and the linewidth ratio, we had limited success. In Figure 6 we plot the relation between the linewidth ratio, Hα equivalent width, and concentration index; NGC 4449 is plotted as a comparison object. Only the lower panel shows any hint of a correlation: objects with higher EW(Hα) seem to have lower linewidth ratios, while those lower EW(Hα) have a wider range of ratios. The relation, really an upper envelope, between EW(Hα) and $\mathcal{R}$ may indicate that galaxies undergoing a large starburst have small linewidth ratios. Physically, this could be caused by a minor merger driving some gas into the center of a galaxy, triggering a central starburst (e.g. Hernquist & Mihos 1995). Therefore, most of the line emission will be centrally concentrated, while the H I disk will be more extended. Such a starburst cannot dominate the optical light, however, since there is no correlation between the linewidth ratio or EW(Hα) and concentration index. Alternatively, some of the H I gas could be in the process of being ejected from the galaxy and is no longer tracing the gravitational potential. This would require very large amounts of mass to be ejected without being ionized. Furthermore, the shapes of most of the H I profiles can be more simply explained by galactic rotation than by ejection.

5.2. Neutral Gas Masses and the Potential For Future Star Formation

The 10 galaxies with 21 cm detections have H I masses ranging from 0.26-4.3×10^9 $M_\odot$. This H I mass range is typical for later-type spiral (Sc-Sm) and irregular galaxies (Roberts & Haynes 1994). The SFRs of our 10 sample galaxies range between 0.23-23.5 $M_\odot$ yr^{-1}. Thus, our samples spans a wide range of H I masses and Hα luminosities (or SFR) similar to the heterogeneous sample of spiral galaxies studied by Kennicutt, Tamblyn, & Congdon (1994; KTC) as shown in Figure 7. The gas depletion timescales for our sample galaxies are also similar to the KTC sample, with typical $\tau_{gas} > 1$ Gyr, also shown in Figure 7. Only 3-4 galaxies in our sample have τ_{gas} less than 1 Gyr: UCM 0040+0220, UCM 0148+2123, UCM 2325+2318, and UCM 2351+2321. These are not anomalously low for KTC spirals, but are on the lower edge of the distribution. The cause of these low τ_{gas} values is either having a small H I mass and a moderate SFR (e.g. UCM 0040+0220 and UCM 0148+2123), or a high SFR and moderate $M_{H\ I}$ (e.g. UCM 2325+2318), or a combination of high SFR and low $M_{H\ I}$ (e.g. UCM 2351+2321).

From the inclination-corrected H I linewidths, we estimate the dynamical mass of each system

using $R_{\rm H\ I}$ as a fiducial radius. The masses range from 3.7×10^9 $M_\odot$ to 1.5×10^{10} $M_\odot$. It should be noted that the derived inclinations can be highly uncertain ($\pm 15°$), and produce large corrections to the H I linewidths for low inclinations. Such errors in inclination propagate into our mass determination as the square of the linewidth. If our estimate of $R_{\rm H\ I} = 4.5\ R_{eff}$ is too large, then the dynamical masses should be reduced in proportion to $R_{\rm H\ I}$.

Using our derived M_{dyn} and calculated $M_{\rm H\ I}$ we can calculate the neutral hydrogen gas mass fraction, f_{gas}. The gas mass fractions for our sample have reasonable values that range from 0.01 to 0.54 with a mean value of 0.12. Thus, some of these galaxies may be gas rich like nearby H II and irregular galaxies ($f_{gas} \sim 0.3 - 0.5$; Van Zee, Salzer & Skillman 1998) while others could have gas mass fractions typical of the Milky Way and other spirals ($f_{gas} < 0.10$; Roberts & Haynes 1994).

There are some ambiguities in the interpretation of H I profiles worth consideration. Our estimates of H I masses may be too large if there are multiple galaxies in the relatively large Arecibo beam (90 kpc in extent at an average distance of 83 Mpc). Multiple galaxies are not necessarily easy to identify from a spatially integrated H I profile. They can produce asymmetric single or doubly peaked profiles, and/or flat or rounded-top H I profiles (see Nordgren *et al.* 1997a, 1997b for examples). Depending on the masses and dynamics of the system, the asymmetries may be quite small, even if the relative masses are high. An overestimate of the H I masses would result in an overestimate of τ_{gas}. Therefore, these galaxies may be using up their H I at a more prodigious rate than indicated by the present estimates. Finally, it is difficult to determine if interactions are ongoing in the sample galaxies from the H I profiles. Interactions will affect the observed linewidths, and, hence, the accuracy of our calculated dynamical masses. Strong single peaks are predicted and seen in some merger remnants (Horellou & Booth 1997; Bendo & Barnes 2000), but other interacting systems or merger remnants are indistinguishable from normal, isolated galaxies (Horellou & Booth 1997). Only with higher spatial resolution H I observations can these ambiguities be cleared up. For this paper we can only assume that we have observed single galaxies.

5.3. Comparison to Intermediate Redshift Blue Compact Galaxies

Over the last few years, there has been an increasing controversy surrounding the reliability of the virial mass estimates using velocity widths measured from ionized gas emission in BCGs at intermediate redshifts. It is well known that the ionized gas does not always sample the whole range of the rotation curve, since the space distribution of the ionized gas is typically more compact than the extended HI (e.g., Broeils 1992; Taylor et al. 1995). Velocity widths derived using ionized gas emission lines likely underestimate the actual galaxy gravitational potential, and thus the inferred virial mass. The key question is: "How do we relate optical line-widths to the rotation velocity?" Since emission line velocity widths are often used to estimate galaxy masses in unresolved BCGs at higher redshifts, it is important to assess the degree at which these measurements may be biased by a likely underestimation of the actual rotation velocity.

For BCGs at redshift $z < 0.35$, the issue was first discussed by Guzmán et al. (1996) who re-analyzed $\mathcal{R}$ in the published data for a sample of nearby HII galaxies (Telles & Terlevich 1992) and concluded that "since CNELGs are similar to H II galaxies, the measured velocity widths are likely to underestimate their internal velocities by as much as 30%". A 30% increase was thus applied to velocity widths measurements in subsequent papers (e.g., Guzmán et al. 1998). The value of this correction was also investigated by Rix et al. (1997) who compared the velocity dispersion in the ionized gas, σ_v, with the maximum circular velocity of the ionized gas, V_c, for three, well-resolved, nearby galaxies. They found an average value of $\sigma_v/V_c = 0.6$ which is consistent with the analytic prescription of Tully & Fouqué (1985). On the other hand, Lehnert & Heckman (1996) showed a very poor correlation between emission line velocity widths and rotational velocities for a sample of local starburst galaxies (see their figure 13). They noted that emission lines from nuclear regions trace only a fraction of the rising portion of the rotation curve in nuclear starbursts, but they did not investigate how this affected the spatially-integrated optical spectrum of the galaxy, or how global optical linewidths compared to the H I linewidths. Neither Rix et al. (1997) nor Lehnert & Heckman (1996) discussed the relation of the ionized gas kinematics to the neutral gas kinematics, which is the issue of interest here. Kobulnicky & Gebhardt (2000) performed integrated optical spectroscopy of 21 galaxies, including some of the Lehnert & Heckman (1996) nuclear starburst sample, and they found good agreement between optical and H I linewidths for all objects except NGC 4449. Note that NGC 4449 is the object in the Kobulnicky & Gebhardt (2000) sample that most closely resembles the BCG population.

In order to assess the relevance of our work for distant galaxies, it is important to consider how analogous our sample of 11 galaxies is to the intermediate redshift BCGs that we wish to learn more about. We can examine how our sample galaxies compare in the M_B–$\sigma_{\rm H\ II}$ and R_{eff}–$\sigma_{\rm H\ II}$ planes. In Figure 8 we compare the distribution of our sample galaxies to the BCGs of Phillips et al. (1997) and Guzmán et al. (1998). While our galaxies span nearly the full range of M_B and R_{eff} as the distant BCGs, they have systematically smaller linewidths. Indeed, the nearby sample shows a mean emission line velocity width near 30 $km\ s^{-1}$ compared to 50-60 $km\ s^{-1}$ for the BCGs; both sets of linewidths are uncorrected for inclination. Figure 8 brings into question whether we are truly observing analogs to the intermediate redshift BCGs. We believe, however, that our sample galaxies, while not representative of all intermediate redshift BCGs, are similar to those with the smallest linewidths (i.e., $\sigma < 40\ km\ s^{-1}$).

The hypothesis that we are observing analogs to at least some of the intermediate redshift BCGs is supported by examining other morphological and photometric properties of our galaxies. In Figure 9, we plot the $B - V$ colors versus asymmetry, A, concentration index, C, and B-band surface brightness with the half-light radius, SBe, for our sample galaxies, the Frei (1999) sample of local, luminous elliptical and spiral galaxies with parameters measured by Bershady et al. (2000), the luminous BCG sample from Jangren et al. (2001), and the BCG sample from the HDF-ff with parameters measured by Guzmán et al. (1997). With the exception of two red sources (UCM0159+2354 and UCM2351+2321), our galaxies occupy a location in the $B - V$ vs. SBe and

$B-V$ vs. C planes that overlaps strongly with the intermediate redshift BCG samples and is clearly distinct from normal, nearby galaxies. Most of the galaxies in our sample are less luminous and redder than the majority of the intermediate redshift BCGs. Based on the definition of BCGs from Jangren et al. (2001) 7 of our 11 galaxies are "BCGs" (the exceptions are UCM 0148+2124, UCM 0159+2354, UCM 2329+2512, and UCM 2351+2321). Of those seven, only the three most luminous galaxies in our sample technically fit the "LBCG" definition of Jangren et al. (2001) (UCM 2325+2318, UCM 0135+2242, and UCM 2251+2352). All of these points serve to illustrate that we must be very careful about what we infer regarding the nature of intermediate redshift BCGs based on observations of our sample of galaxies or similar samples in the local universe. For instance, the two nearby galaxies Barton & van Zee (2001) propose are local counterparts to the intermediate redshift BCG population would not have been selected as such by the color - surface brightness criteria defined by Jangren et al. (2001). These two nearby galaxies are either redder or of lower surface brightness (or both) than the intermediate redshift BCGs as well as the nearby sample studied here. With this caveat in mind, we will now examine what we can learn about intermediate redshift BCGs.

At the top of Figure 5, we have drawn several boxes to represent the range of linewidths for the galaxies in the studies of the Hubble Deep Field flanking fields (Phillips et al. 1997), z∼0.6 field galaxies (Mallén-Ornelas et al. 1999), z∼0.25 field galaxies (Rix et al. 1997) and compact blue galaxies at z∼0.4 (Guzmán et al. 1998). Figure 5 shows that the discrepancy between H II and H I linewidths described in Section 4.1 could affect the mass determinations in all these studies. The effect can be as much as a factor of 2-4 for the smallest velocity width galaxies. However, according to our empirical relation, the effect may be only ∼30-40% for galaxies with velocity widths $\sigma > 40$ km s^{-1}. Note that this effect is in addition to other well-recognized uncertainties in mass determinations due to unknown inclinations and clumpy gas distributions (modeled for spiral galaxies by Rix et al. 1997). A more rigorous approach to apply the results from our study to the intermediate redshift BCG population is to restrict our conclusions only to the seven galaxies that can be considered "bona fide" counterparts according to Jangren et al.'s definition. These galaxies have a $\mathcal{R}$ ranging from 0.54 to 0.94, with a mean value of 0.70. The three "bona fide" LBCG counterparts have essentially the same mean and range. For the 3 non-BCG galaxies we detected in H I the mean value of $\mathcal{R}$ is only 0.54. These values of $\mathcal{R}$ for BCGs are in good agreement with the corrections applied to the mass estimates in previous work at higher redshift (e.g., Guzmán et al. 1996, 1998).

One of the most interesting conclusions derived using mass estimates of BCGs at intermediate redshifts is that their mass-to-light ratios are roughly one order of magnitude lower than those values characteristic of local galaxies with similar luminosities (Guzmán et al. 1996; Phillips et al. 1997). This conclusion can be tested with our sample of nearby BCGs. For consistency with previous work, we define the mass-to-light ratio within R_{eff} (instead of R_{HI}), using the velocity dispersion of the H I and uncorrected by inclination effects. This definition allows a direct comparison with values published in the literature for a wide variety of galaxy types. For our entire sample, the derived

mass-to-light ratios range from 0.07 to 0.78 $M_\odot/L^B_\odot$. The mean mass-to-light ratio for non-BCGs, 0.6 $M_\odot/L^B_\odot$, is higher than for the BCGs, 0.3 $M_\odot/L^B_\odot$, in our sample. These values are consistent with the mass-to-light ratios for intermediate redshift BCGs studied by Phillips et al. (1997). The mean absolute magnitude is $M_B = -19.2$ mag; about 1.3 magnitudes fainter than L$\star$. Using the same representative sample of local galaxies in the RC3 (de Vaucouleurs et al. 1991) analyzed by Phillips et al. (1997), we estimate that nearby, "normal" galaxies with $M_B \sim -19.2$ have mass-to-light ratios that approximately range from 0.8 to 10 $M_\odot/L^B_\odot$. The observed range in mass-to-light ratio for BCGs inconsistent with that characteristic of massive systems with comparable luminosities, such as Sa-Sc spiral galaxies. These spirals tend to be the most abundant galaxy type with this luminosity in the local universe. Instead, BCGs have mass-to-light ratios that are similar to the lowest observed values in lower-mass galaxies of similar luminosity, such as irregulars and HII galaxies. As our BCG counterparts evolve, their mass-to-light ratios will increase to values more comparable to normal, spiral galaxies, provided that they fade.

Finally, the observed distribution of gas depletion timescales τ_{gas} provides additional information about the nature and evolution of the distant BCG galaxy population. Of the seven BCGs in our sample, two have $\tau_{gas} < 0.5$ Gyrs, two have $\tau_{gas} \sim 1$ Gyrs, and three have $\tau_{gas} > 2$ Gyrs. The wide range observed suggests a very heterogeneous population of objects with very different burst strengths and reservoirs of neutral gas. The BCGs with the smallest gas depletion timescales will shortly cease star formation and thus may be good candidates to undergo subsequent passive evolution. However, a long period of passive evolution following the end of the current starburst in BCGs with $\tau_{gas} > 2$ Gyr seems less likely and these galaxies may continue having subsequent events of star formation.

5.4. Implications for the Evolution of the Tully-Fisher Relation

A related controversy exists concerning whether velocity widths of ionized gas are suitable for the study of galaxy scaling relations such as the Tully & Fisher relation (1977; T-F). Traditionally, the T-F relation is a correlation measured between luminosity and HI line-width. It has been well established that "terminal" rotation speeds derived from spatially resolved velocity fields (in the optical or HI) provide a well-defined surrogate for HI line-widths for normal spiral galaxies in the local universe (e.g., Mathewson et al.1992, Courteau 1997). Ionized gas line-widths are of particular interest for intermediate- and high-redshift work where spatial resolution and signal-to-noise are limited and HI is out of reach with present telescopes and instrumentation. However, there has been only limited exploration of whether optical *line-widths* are suitable surrogates for use in measuring the T-F relation (e.g., Rix et al. 1997; KG00). Despite this fact, there have been a number of studies attempting to exploit the observability of optical line-widths for drawing inferences about the evolution of M/L of intermediate-redshift galaxies, as discussed in the Introduction. Our purpose here is to demonstrate that these results should be viewed with caution.

Figure 10 shows how our sample of compact galaxies compares to the T-F relation. Each

galaxy in our sample is plotted three times. Dotted circles denote the measured H II linewidths, W_{20}(H II), circles denote the measured H I 21-cm linewidths, $W_{20}(HI)$, and filled circles denote the inclination-corrected H I 21-cm linewidths, $W_{20}(HI)/sin(i)$. For comparison, we also plot H II galaxies from Telles & Terlevich (1993; crosses), and the B-band Tully-Fisher relation of Pierce & Tully (1988; solid line).[7] While the compact galaxies in our sample lie near the relation for H II galaxies and show a large offset from the canonical T-F relation when using observed H II line-widths, if we we adopt the inclination-corrected H I widths our sample is consistent on average with the T-F relation for normal galaxies.

Prompted by this result, we have re-examined the results of T-F studies at intermediate redshift employing line-widths. Specifically, we have re-computed magnitude offsets from T-F for the Forbes et al. (1996), Rix et al. (1997), and Mallén-Ornelas et al. (1999) samples after applying the line-width correction in Equation 3 (Figure 5). The line-widths of the Forbes et al. sample are such that corrections based on our formulation are minimal, despite the discussion noted above based on their own rotation curve data. Indeed, it is sobering to note that of the two galaxies for which they have rotation curves, the galaxy with the small line-width correction appears to have a bimodal light distribution, while the galaxy with the large line-width correction appears to be a relatively normal spiral with large luminosity and size (see their figure 1).

For Rix et al. we use their tabulated line-widths and adopt the Pierce & Tully (1988) T-F relation, which has a slope of $\gamma = -6.86$. The adopted slope is within 1σ of the value derived by Rix et al. (1997) for their intermediate-redshift sample; ours is a conservative choice since their mean slope is much steeper ($\gamma = -14.3$) and hence results in much larger magnitude-offset corrections. We find a mean offset of -1.8 mag without applying line-width correction. This is -0.3 mag larger than their quoted mean value, consistent with our ignoring the color-dependence to the T-F zeropoint (see their §3.3.1, eqn. 9). However, with line-width corrections we find a mean offset of -1.1 mag, or +0.7 mag less brightening than estimated by Rix et al. (1997). Accounting for their color-dependence results in a net, corrected brightening of -0.8 mag in the T-F zeropoint at $z \sim 0.25$.

To make a fair re-assessment with Mallén-Ornelas et al.'s results, we adopt their T-F slope of $\gamma = -7.46$. Since Mallén-Ornelas et al. (1999) do not provide tabulated data nor a zeropoint for their fiducial T-F relation, we estimate a correction for their median line-width (60 $km\ s^{-1}$)

---

[7] $M_B = -6.86 \log(V_M) - 2.27$. In order to convert V_M to the observed quantity, W_{20}, we adopt the prescription of Tully & Fouqué (1985),

$$(2 \times V_M)^2 = W_R^2 = W_{20}^2 + W_t^2 - 2W_{20}W_t[1 - e^{-(W_{20}/W_c)^2}] - 2W_t^2 e^{-(W_{20}/W_c)^2}. \quad (4)$$

W_R is the rotation full amplitude which is $2\times V_M$. $W_t = 38\ km\ s^{-1}$ is the width due to turbulent motions and $W_c = 120\ km\ s^{-1}$ is the transition point between galaxies having Gaussian and those having double-horned H I profiles.

estimated from their figure 2, and calculate a differential correction, ΔM_c, given as:

$$\Delta M_c = -\gamma \log(\frac{W_{\rm H\ II}}{W_{\rm H\ I}}), \tag{5}$$

where the linewidth ratio is given by our Equation 3. We find a median correction is +0.2 mag, although we note that at the lower line-width limit of their sample the correction is +1.9 mag, which is comparable (but opposite in sign) to their average estimated brightening.

In isolation, the picture that emerges from this re-analysis of intermediate redshift line-width studies is that the evolution of the T-F zeropoint is more gradual than previously suggested – even for the bluest galaxies studied by Rix et al. (1997) and Mallén-Ornelas et al. (1999). For these galaxies we estimate -0.8 mag at $z \sim 0.25$ and -1.8 mag at $z \sim 0.6$. However even this revised estimate should still be tempered by the fact that corrections for color-dependence in the T-F relation relation and inclination are uncertain. For example, the color-dependence of the T-F zeropoint estimated by Rix et al. is ∼3 times smaller than what is reported in Bershady et al. (2001). In the absence of direct inclination measurements (e.g., b/a), Rix et al. (1997) have performed an elegant estimate of the mean inclination of their sample. They take into account that the bluest galaxies may preferentially lie at relatively low inclinations (where internal reddening is minimized). However, our sample's mean inclination is 43°, with a maximum of 60°; almost all of our sample is more face-on than the mean inclination of $\sim 57°$ adopted by Rix et al. (1997). If our sample is representative of the inclination distribution of the blue galaxy population, taking into account this change in mean projection results in +0.6 mag less brightening (assuming $\gamma = -6.86$). Similarly, Mallén-Ornelas et al. (1999) compare their uncorrected velocities for intermediate redshift galaxies to a local sample from the RC3. While they make identical cuts in b/a (< 0.8), the two samples may not have comparable inclination distributions. Our arguments here are admittedly tentative, and are not intended to diminish the pioneering efforts to measure the T-F relation at intermediate redshifts. Yet the striking fact remains that most intermediate-redshift studies employing spatially-resolved rotation curves find less evolution (e.g., Vogt et al.1996, 1997; Bershady et al. 1999), and that by using the inclination-corrected H I linewidths even the galaxies studied in this paper fall squarely on the local T-F relation.

A corollary to the result in Figure 10 is that our local sample of BCGs cannot fade nor brighten dramatically *and* remain on the T-F relation. The relatively large reservoir of gas in most of these systems indicates these galaxies will likely experience star-formation in their future, as discussed in previous sections. However the amplitude of past and future star-formation is not well constrained, and so the basic assumption that these systems remain (or have been) on the T-F relation is weak. Analogous galaxies at intermediate redshift also will be so weakly bound. Nonetheless, if we assume these galaxies have remained on the T-F relation (or brighter) over lifetimes in excess of 5 Gyr, then the current burst makes only a small contribution to the total stellar mass. Consequently, in this scenario these galaxies also are not candidates for strong fading in the future.

However, it is important to stress that the extant characteristics of the local galaxies studied here are dissimilar to the extreme LBCGs for which a strong fading scenario was originally proposed

by Koo et al. (1995) and Guzmán et al. (1996). The fading these authors postulated was part of a transformation process whereby some subset of the LBCGs evolved into today's spheroidals. As such, these LBCGs would not be expected to lie or remain on the T-F relation at any time. In other words, the assumption that these galaxies must remain on the T-F relation, made in the previous paragraph, is not valid in this scenario.

Finally, the trends of our line-width ratio, $\mathcal{R}$, with line-width also has implications for the line-widths of Lyman Break galaxies (LBGs) observed at z>2.7 (e.g., Pettini et al. 2001). Pettini et al. are skeptical of whether their ionized gas line-widths are tracing mass. They note, for instance, that they find little evidence for a line-width luminosity relation in their sample or in a larger sample at z∼1. The effect of the line-width dependence of $\mathcal{R}$ will be to decrease the slope of the T-F relation, as shown in Figure 10. While the effect is rather mild in Figure 10, it may be more extreme for galaxies at higher redshift. It is striking that while the LBGs are 1-3 magnitudes brighter than the intermediate redshift LBCGS, they have comparable range of ionized-gas velocity widths, with mean values of 70 and 60 $km\ s^{-1}$ respectively. Indeed, the gas content of galaxies is presumably larger at higher redshifts, and hence it may be reasonable to expect that the value and trend of $\mathcal{R}$ with line-width evolves and becomes more extreme at higher redshift. We share, then, Pettini et al.'s caution in interpreting their ionized gas line-widths, but remark that our corrections should at least provide a lower limit to what should be applied to the ionized gas line-widths at high redshift.

6. Conclusions

The present sample of compact galaxies were chosen to be analogous to the Blue Compact Galaxies (BCGs) at intermediate redshift, so that we could infer the gaseous properties of such galaxies. For our sample, we find that the neutral hydrogen masses, hydrogen gas mass fractions, star formation rates, and gas depletion timescales are comparable to nearby gas-rich spiral, irregular and HII galaxies. The broad range of HI properties imply BCGs form a very heterogeneous galaxy class. Our sample galaxies have substantial amounts of neutral hydrogen ($\sim 10^9$ $M_\odot$) and large inferred total masses ($\sim 10^{10}$ $M_\odot$). However, unlike most nearby, luminous spiral and irregular galaxies, the ratio of H II to H I linewidths, $\mathcal{R}$ is systematically less than unity with a mean value near 0.66. In this respect our sample is similar to nearby H II galaxies. The magnitude of $\mathcal{R}$ is close to what was assumed by Guzmán et al. (1998) and others for intermediate redshift BCGs. In addition, $\mathcal{R}$ varies with H II linewidth, departing dramatically from unity for W_{20}(H II) ≤ 200 $km\ s^{-1}$. We have parameterized this relationship to help those who wish to attempt a correction in higher redshift data. Unfortunately, there is no tight correlation between any of the morphological or photometric properties of these galaxies and the linewidth ratio, $\mathcal{R}$. The upper limit of $\mathcal{R}$ does appear to decrease with increasing Hα equivalent width, suggesting that this effect is related to central starbursts in these galaxies, but this is tenuous conclusion. Applying the corrections due to inclination and converting from H II to H I linewidth for our galaxies moves them onto the

Tully-Fisher relation, leaving little room for these galaxies to fade if they are to remain on the relation. This implies that the evolution of the Tully-Fisher relation from intermediate redshift to the present day is smaller and more gradual than has been previously been suggested (e.g., Rix et al. 1997).

Although the luminosities, colors, and effective sizes of our sample were chosen to mimic those of the BCG population at intermediate redshifts, our sample remains heterogeneous and only samples a portion of the properties of BCGs. Of the 11 galaxies we observed, only 7 can be classified as BCGs based on the definition of Jangren et al. (2001). Only the brightest 4 of those 7 BCGs are classified as LBCGs. Furthermore, our galaxies have systematically smaller linewidths than the observed population of intermediate redshift BCGs. They also tend to have, on average at a given luminosity, smaller sizes. Therefore our sample is not representative of all intermediate redshift BCGs, but only a subset of them. As such, we are limited in what we can infer regarding the properties of the distant BCGs. For those intermediate redshift BCGs with small velocity widths and sizes, we can assume that they will form also a heterogeneous population of relatively gas rich galaxies ($\sim 10^9$ $M_\odot$) whose gas fractions ($f_{gas} = 0.02 - 0.5$) and gas depletion timescales ($\tau_{gas} = 0.2 - 6$ Gyrs) may span well over one order of magnitude. Although it is not possible to constrain the evolutionary descendants of these BCGs from the present data, we can remark that the relatively large dynamical and H I masses measured for about two-thirds of our sample will function to inhibit the ejection of the ISM and to fuel future star formation. Although the current bursts of star formation are strong, they are unlikely to be the last, nor may they produce the dominant stellar population in many of these galaxies. The remaining one-third of our sample shows, however, gas depletion timescales short enough to suggest that they may cease star formation in the near future and thus may be good candidates to undergo subsequent passive evolution.

Future work on this topic is essential. Higher spatial resolution H I data will help us resolve any confusion regarding the interpretation of our single-dish observations. It will also allow us to probe the internal structure of these galaxies to better understand how the effects of interactions may be affecting our calculated masses. Observations of the molecular gas in these galaxies will help determine the total gas mass available for star formation in these galaxies. Finally, observations of a much larger sample which is more representative of the BCG class at intermediate redshift is necessary to better infer the properties of their distant counterparts. This is the only way to divine the gaseous properties of the intermediate redshift BCGs until we are capable of observing them directly.

7. Acknowledgments

We wish to thank the staff at the Arecibo Observatory for all their assistance and hospitality during our observations there. They helped make the observing run both enjoyable and successful. Special thanks to Snezana Stanimirovic, our "friend" at Arecibo, who went above and beyond

the call of duty in helping us prepare for observing, observe, and reduce the data. We thank P.G. Pérez-Gonzalez for providing B magnitudes and B-r colors for our sample galaxies. We also thank John Salzer, Liese van Zee, and David Koo for their comments which helped improve the manuscript. The Digitized Sky Surveys were produced at the Space Telescope Science Institute under U.S. Government grant NAG W-2166. The images of these surveys are based on photographic data obtained using the Oschin Schmidt Telescope on Palomar Mountain and the UK Schmidt Telescope. The Second Palomar Observatory Sky Survey (POSS-II) was made by the California Institute of Technology with funds from the National Science Foundation, the National Geographic Society, the Sloan Foundation, the Samuel Oschin Foundation, and the Eastman Kodak Corporation. D.J.P. acknowledges partial support from the Wisconsin Space Grant Consortium. H.A.K. is grateful for support from Hubble Fellowship, HF-01094.01-97A, award by the Space Telescope Science Institute. R.G. acknowledges support from Hubble Fellowship, HF-01092.01-97A, award by the Space Telescope Science Institute. J.G. acknowledges partial support form the Spanish Programa Sectorial de Promoción del Conocimiento under grant PB96-0645. M.A.B. acknowledges for support from NSF grant AST-9970780 and LTSA contract NAG5-6032.

REFERENCES

Alonso-Herrero, A., Aragón-Salamanca, A., Zamorano, J., & Rego, M., 1996, MNRAS, 278, 417

Aaronson, M., Huchra, J., & Mould, J. 1980, ApJ, 237, 655

Barton, E.J., & van Zee, L., 2001, ApJ, 550.

Bendo, G.J., & Barnes, J.E., 2000, MNRAS, in press

Bershady, M. A. 1997, in "Dark and Visible Matter in Galaxies and Cosmological Implications," eds. M. Persic and P. Salucci (ASPCS), 117, 547

Bershady, M. A. & Andersenn, D. A. 2001, to appear in "Galaxy Disks and Disk Galaxies," eds. J.G. Funes, S.J. and E.M. Corsini (ASPCS), astro-ph/0010118

Bershady, M. A., Haynes, M. P., Giovanelli, R., Andersen, D. R. 1999, in "Galaxy Dynamics," eds. D.R. Merritt, M. Valluri, J.A. Sellwood (ASPCS), 182, 499

Bershady, M. A., Jangren, A., & Conselice, C. J. 2000, AJ, 119, 2645

Broeils, A.H., 1992, Ph.D. Thesis, University of Groningen

Conselice, C.J., Bershady, M.A., & Gallagher, J.S., A&A, 354, L21.

Courteau, S. 1997, AJ, 114, 2402

Ellis, R.S., 1997, ARA&A, 35, 389

Frei, Z. 1999, Ap&SS, 269, 649

Forbes, D. A., Phillips, A. C., Koo, D. C., Illingworth, G. D. 1996, ApJ, 462, 89

Gallego, J., Zamorano, J., Rego, M., Alonso, O., Vitores, A.G. 1996, A&AS, 120, 323

Gallego, J., Zamorano, J., Rego, M., Vitores, A.G. 1997, ApJ, 475, 502

Guzmán, R., Koo, D. C., Faber, S. M., Illingworth, G. D., Takamiya, M., Kron, R. G., & Bershady, M. A. 1996, ApJ, 460, L5

Guzmán, R., Gallego, J., Phillips, A., Koo, D., Lowenthal, J.D., Faber, S.M., Illingworth, G., Vogt, N. 1997, ApJ, 489, 559.

Guzmán, R.,Jangren, A., Koo, D. C., Bershady, M. A. & Simard, L. 1998, ApJ, 495, L13

Horellou, C., & Booth, R., 1997, A&AS, 126, 3

Homeier, N. L., Gallagher, J.S., 1999, ApJ, 522, 199

Jangren, A., Bershady, M. A., Conselice, C. J., Koo, D. C., & Guzmán, R. 2001, ApJ, submitted

Kennicutt, R.C., 1983, ApJ, 272, 54

Kennicutt, R.C., Tamblyn, P., & Congdon, C.E., 1994, ApJ, 435, 22 (KTC)

Kobulnicky, H. A. & Gebhardt, K., 2000, AJ, 119, 1608 (KG00)

Koo, D. C., Bershady, M. A., Wirth, G. D., Stanford, S. A., & Majewski, S. R. 1994, ApJ, 427, L9

Koo, D. C., Guzmán, R., Faber, S. M., Illingworth, G. D. Bershady, M. A., Kron, R. G., & Takamiya, M. 1995, ApJ, 440, L49

Lehnert, M.D., Heckman, T.M., 1996, ApJ, 462, 651

Lowenthal, J. D., Koo, D. C. Guzmán, R., Gallego, J., Phillips, A. C., Faber, S. M., Vogt, N. P., Illingworth, G. D., Gronwall, C. 1997, ApJ, 481, 673

Mallén-Ornelas, G., Lilly, S. J., Crampton, D., & Schade, D. 1999, ApJ, 518, L83

Mathewson, D. S., Ford, V. L., Buchhorn, M. 1992, ApJS, 81, 413

Nordgren T.E., Chengalur, J.N., Salpeter, E.E., & Terzian, Y., 1997a, AJ, 114, 77

Nordgren T.E., Chengalur, J.N., Salpeter, E.E., & Terzian, Y., 1997b, AJ, 114, 913

Pérez-González, P.G., Zamorano, J., Gallego, J., Gil de Paz, A. 2000, A&A, 141, 409

Pettini, M., Shapley, A.E., Steidel, C.C., Cuby, J.-G., Dickinson, M., Moorwood, A.F.M., Adelberger, K.L., & Giavalisco, M., 2001, ApJ, 554, in press

Phillips, A.C., Guzmán, R., Gallego, J., Koo, D.C., Lowenthal, J.D., Vogt, N.P., Faber, S.M., & Illingworth, G.D., 1997, ApJ, 489, 543

Pierce, M. J., & Tully, R. B. 1988, ApJ, 330, 579

Rix, H.-W., Guhathakurta, P., Colless, M., & Ing, K., 1997, MNRAS, 285, 779

Raychaudhury, S., von Braun, K., Bernstein, G., Guhathakurta, P. 1997, AJ, 113, 2046

Roberts, M.S., & Haynes, M.P., 1994, ARA&A, 32, 115

Sanders, D.B., & Mirabel I.F., 1996, ARA&A, 34, 749

Schade, D., Lilly, S. J., Crampton, D., Hammer, F., Le Fevre, O., Tresse, L. 1995, ApJ, 451, 1

Simard, L. and Pritchet, C. J. 1998, ApJ, 505, 96

Smoker, J. V., Davies, R. D., Axon, D. J., & Hummel, E. 2000, A&A, 361, 19

Steidel, C. C., Giavalisco, M., Pettini, M., Dickinson, M., & Adelberger, K. L. 1996a, ApJ, 462, L17

Steidel, C. C., Giavalisco, M., Dickinson, M., & Adelberger, K. L. 1996b, AJ, 112, 352

Telles, E., & Terlevich, R., 1993, ApSS, 205, 49

Tully, R. B., & Fisher, J. R. 1977, A&A, 54, 661

Tully, R. B., & Fouque, P. 1985, ApJS, 58, 67

Vitores, A.G., Zamorano, J., Rego, M., Alonso, O., & Gallego, J., 1996a, A&AS, 118, 7

Vitores, A.G., Zamorano, J., Rego, M., Gallego, J. & Alonso, O., 1996b, A&AS, 120, 385

Vogt, S.S., *et al.*, 1994, Proc. SPIE, 2198, 362

Young, L.M., 2000, AJ, 119, 188

Young, L.M., & Lo, K.Y., 1997, ApJ, 490, 710

van Zee, L., Skillman, E.D., & Salzer, J.J., 1998, AJ, 116, 1186

Vogt, N. P., Forbes, D. A., Phillips, A. C., Gronwall, C., Faber, S. M., Illingworth, G. D., Koo, D. C. 1996, ApJ, 465, L15

Vogt, N. P., Phillips, A. C., Faber, S. M., Gallego, J., Gronwall, C., Guzmán, R., Illingworth, G. D., Koo, D. C., Lowenthal, J. D. 1997, ApJ, 479, L121

Zamorano, J., Rego, M., Gallego, J., Vitores, A.G., González-Riestra, R., Rodriguez-Caderot, G., 1994, ApJS, 95, 387

Zamorano, J., Gallego, J., Rego, M., Vitores, A.G., Alonso, O. 1996, ApJS, 105, 343

This preprint was prepared with the AAS LaTeX macros v5.0.

Table 1. Targets

Name	RA (1950) ^{h} ^{m} ^{s}	Dec. (1950) ^{o} $'$ $''$	Obs. Time min.	Notes
UCM0014+1829	00:14:39.9	18:29:38	18	···
UCM0040+0220	00:40:15.6	02:20:24	24	UM 63
UCM0056+0043	00:56:30.2	00:43:53	12	UM 296
UCM0135+2242	01:35:13.6	22:42:04	42	···
UCM0148+2124	01:48:18.5	21:23:53	54	···
UCM0159+2354	01:59:00.5	23:54:44	54	···
UCM2251+2352	22:51:18.9	23:52:14	18	···
UCM2304+1640	23:04:26.2	16:40:02	36	···
UCM2325+2318	23:25:11.9	23:18:49	24	NGC 7673, merger?
UCM2329+2512	23:29:36.1	25:12:09	12	···
UCM2351+2321	23:51:06.8	23:21:16	48	···

Table 2. Line Measurements

Name	RMS mJy/chan	$Vel_\odot$ km s^{-1}	$W_{20}(HI)$ km s^{-1}	$\int Sdv$ Jy km s^{-1}	W_{20}(H II) km s^{-1}	$\mathcal{R}$[1]
UCM0014+1829	1.28	5249±3	204±5	1.15±0.05	117±5	0.57±0.02
UCM0040+0220	1.04	5432±3	136±5	0.18±0.02	96±5	0.65±0.04
UCM0056+0043	1.52	5352±3	133±5	2.1±0.1	126±9	0.94±0.07
UCM0135+2242	1.11	10354±3	249±5	0.83±0.04	225±15	0.90±0.06
UCM0148+2124	0.64	4890±10	200±20	0.32±0.02	98±8	0.49±0.06
UCM0159+2354	0.48	4901±3	192±5	0.52±0.01	138±12	0.71±0.06
UCM2251+2352	1.12	7715±5	140±10	0.60±0.03	79±9	0.56±0.07
UCM2304+1640	0.79	5162±3	157±5	0.99±0.02	85±6	0.54±0.04
UCM2325+2318	1.07	3412±3	164±5	7.21±0.06	119±7[a]	0.72±0.04
UCM2329+2512	1.24	3718±3	203±5	2.50±0.07	88±6	0.43±0.03
UCM2351+2321	0.68	7943±3[b]	···	< 0.042[c]	165±15	···

[1] $\mathcal{R}$= W_{20}(H II)/$W_{20}(HI)$

[a] An independent measurement by N. Homeier (private communication) using WIYN DensePak Hα. observations with a $30'' \times 45''$ integral field yields 126 $km\ s^{-1}$.

[b] Optical velocity from emission lines.

[c] 3σ upper limit over 63 channels (165 $km\ s^{-1}$).

Table 3. Morphological Parameters

Name	Dist (Mpc) (1)	M_B (mag) (2)	B-r (mag) (3)	B-V (mag) (4)	R_{eff} (kpc) (5)	inc (deg) (6)	SBe ($mag/sq\ ''$) (7)	EW(Hα) (Å) (8)	C (9)	A (10)
UCM0014+1829	75	-18.5	0.05	0.16	1.7	50	21.2	146	4.08	0.08
UCM0040+0220	78	-17.7	0.67	0.50	0.6	30	19.9	97	3.00	0.09
UCM0056+0043	76	-18.1	0.42	0.37	0.9	60	20.3	61	2.96	0.07
UCM0135+2242	148	-19.6	0.59	0.46	1.4	45	19.7	60	4.00	0.02
UCM0148+2124	70	-17.7	0.47	0.48	1.0	40	20.9	150	2.72	0.13
UCM0159+2354	70	-17.5	1.00	0.83	1.0	60	21.1	74	4.25	0.12
UCM2251+2352	110	-19.1	0.59	0.47	1.4	15	20.2	84	3.43	0.27
UCM2304+1640	74	-17.1	0.27	0.28	0.7	45	20.6	155	3.35	0.12
UCM2325+2318	49	-20.5	0.30	0.30	1.9	45	19.4	101	2.98	0.60
UCM2329+2512	53	-17.4	0.64	0.49	0.6	45	19.9	160	4.15	0.02
UCM2351+2321	113	-17.8	0.94	0.77	0.7	35	20.1	117	4.02	0.03

[1]Using D(Mpc)=Velocity/H_0; $H_0 = 70\ km\ s^{-1}\ Mpc^{-1}$.

[2]Assumes $H_0 = 70$, $q_0 = 0.05$, from Vitores et al. (1996).

[3]Observed B-r color from Vitores *et al.* (1996); typical uncertainties are 0.12 mag

[4]B-V color derived from the observed B-r color, without correction for redenning, assuming an Irregular galaxy spectral energy distribution, and B-V=0.56(B-r)+0.136 based on Fukugita et al. (1995).

[5]Effective radius in kpc from our WIYN photometry, corrected for the effects of seeing, and assuming the above cosmology.

[6]Inclination, derived from the eccentricity, $e = 1 - b/a$, as in Aaronson, Huchra, & Mould (1980), $i\ (deg) = cos^{-1} sqrt(1.042 * E^2 - 0.042) + 3$ where E=1-e. Typical uncertainties are 15°.

[7]Effective surface brightness, computed from $SB_e = 5 \times \log(R_{eff}(kpc)) + M_B + 38.6$.

[8]$H\alpha$ equivalent width in Å (Gallego et al. 1996)

[9]Concentration index from our WIYN photometry.

[10]Asymmetry parameter from our WIYN photometry.

[a]3σ upper limit for 63 channels ($165\ km\ s^{-1}$).

Table 4. Derived Parameters

Name	$M_{\rm H\ I}$ 10^9 $M_\odot$ (1)	$L_{H\alpha}$ 10^{41} ergs s^{-1} (2)	SFR $M_\odot$/yr (3)	τ_{gas} Gyr (4)	V_{rot} $km\ s^{-1}$ (5)	$R_{\rm H\ I}$ kpc (6)	M_{dyn} 10^{10} $M_\odot$ (7)	f_{gas} (8)	M/L $M_\odot/L_\odot$ (9)
UCM0014+1829	1.52±0.07	1.09	0.98	1.56	133	7.5	2.9	0.05	0.62
UCM0040+0220	0.26±0.03	0.70	0.63	0.41	146	2.9	1.4	0.02	0.20
UCM0056+0043	2.90±0.11	0.51	0.46	6.34	77	4.1	0.5	0.54	0.20
UCM0135+2242	4.32±0.21	1.87	1.68	2.54	177	6.3	4.4	0.10	0.27
UCM0148+2124	0.38±0.02	0.72	0.65	0.59	155	4.5	2.4	0.02	0.71
UCM0159+2354	0.60±0.01	0.53	0.47	1.27	110	4.5	1.2	0.05	0.78
UCM2251+2352	1.78±0.09	1.89	1.70	1.05	270	6.2	10.0	0.02	0.14
UCM2304+1640	1.28±0.03	0.39	0.35	3.65	110	2.9	0.8	0.16	0.53
UCM2325+2318	4.09±0.03	26.3	23.5	0.18	116	8.3	2.5	0.16	0.07
UCM2329+2512	1.66±0.05	0.25	0.23	7.29	144	2.5	1.2	0.14	0.60
UCM2351+2321	< 0.13	1.33	4.53	< 0.03	144[a]	3.2	1.5	$\leq$0.01	0.31

[1]H I mass, $M(\mathrm{H\ I}) = 2.356 \times 10^5\ D^2\ \int\ S\ dv$ [$M_\odot$].

[2]Hα luminosity, from Gallego *et al.* (1996), rescaled to $H_0 = 70$.

[3]Star formation rate, SFR = $\frac{L_{H\alpha}}{1.12\times10^{41}}$, from Kennicutt 1983.

[4]Gas depletion timescale, τ_{gas}=$M_{\rm H\ I}$/SFR, from Kennicutt 1983.

[5]H I rotation velocity corrected for inclination, V_{rot}=0.5×$W_{20}/sin(i)$.

[6]H I radius, $R_{\rm H\ I}$ ∼4.5×R_{eff}, see text for derivation.

[7]Dynamical mass corrected for inclination, M_{dyn}=$V^2_{rot}R_{\rm H\ I}/G$.

[8]f_{gas}=$M_{\rm H\ I}/M_{Dyn}$. Mass of molecular gas and ionized gas not included.

[9]Mass-to-Light ratio at R_{eff}. Mass is calculated from the velocity dispersion, σ=W_{20}(H I)/3.62, without correcting for inclination. Light is the blue luminosity contained within R_{eff} (i.e. half the total luminosity).

[a]from the H II width in Table 2

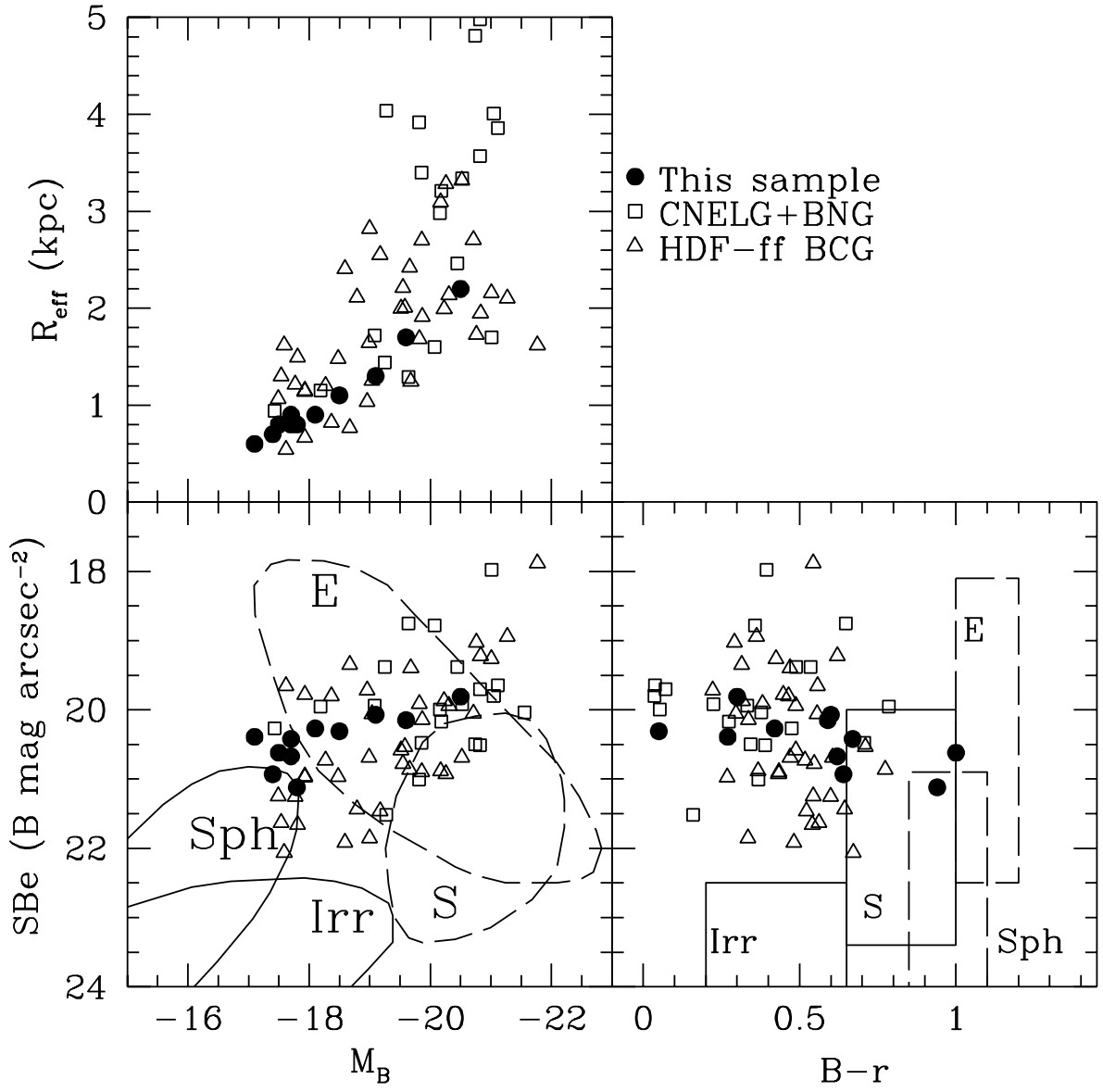

Fig. 1.— A comparison of the selection criteria for 11 UCM sample galaxies (filled circles) with CNELGs and BNGs (squares) from Jangren et al. (2000) and compact galaxies in the HDF flanking fields (triangles) from Phillips *et al.* (1997) and Guzmán *et al.* (1997). The lower left panel shows absolute magnitude vs. B-band surface brightness and includes polygons outlining the general regions where nearby elliptical (E), spiral (S), irregular (Irr), and spheroidal (Sph) galaxies would lie, based on Guzmán et al. (1997). The lower right panel shows color $B-r$ vs. B-band surface brightness (SB_e), with similar polygons. Upper left shows the absolute magnitude versus effective radius, R_{eff}. The sample galaxies have similar luminosities, surface brightnesses and $B-r$ colors as the more distant BCGs.

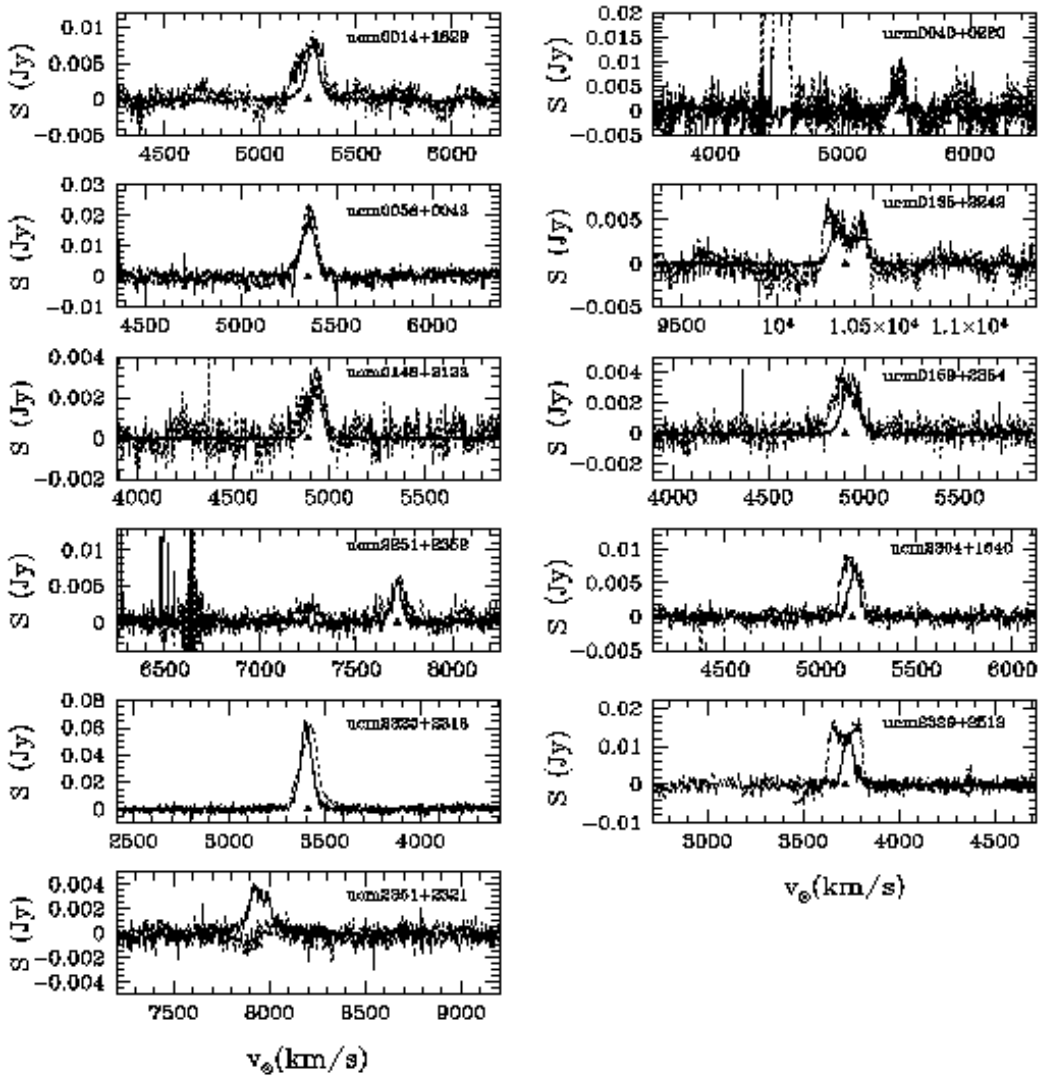

Fig. 2.— H I 21 cm spectra of the sample galaxies plotted as Janskys versus heliocentric recession velocity defined in the optical sense. All but one galaxy is detected. The dark lines are the optical H II emission-line spectra normalized to match the H I Arecibo data in grey. The triangles mark the central velocity of the H I profile. This figure shows good agreement between the systemic

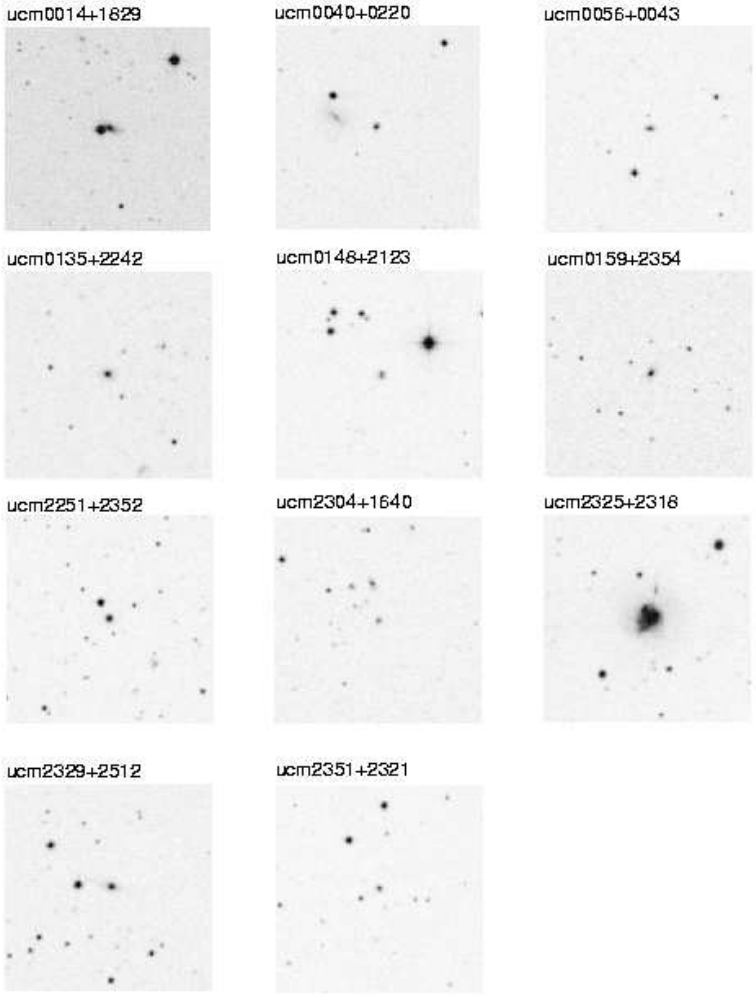

Fig. 3.— Optical images from the Digital Sky Survey centered on the coordinates observed for each galaxy showing a patch of sky 3.′8 on a side to match the largest dimension of the Arecibo beam at 21 cm.

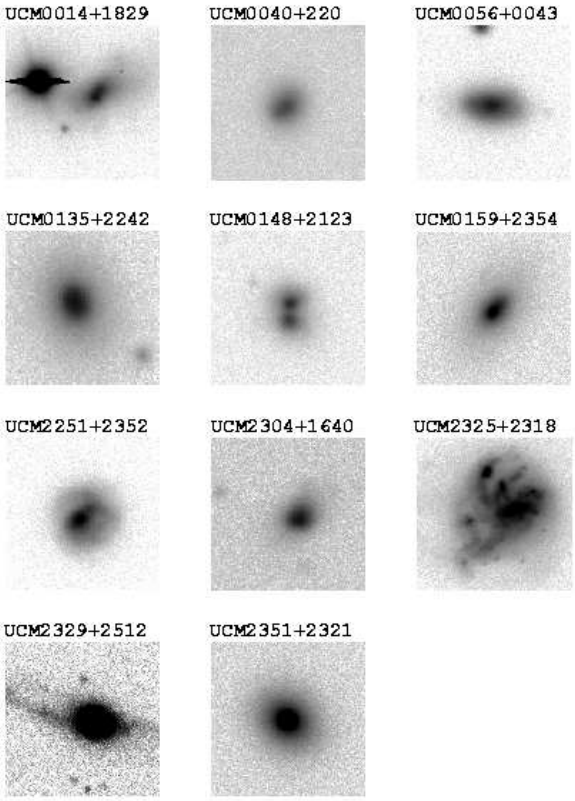

Fig. 4.— R-band logarithmic greyscale images from the WIYN 3.5 m telescope obtained in 1.2″ mean seeing. North is up, and images are 10 kpc on a side at the adopted distance of each source.

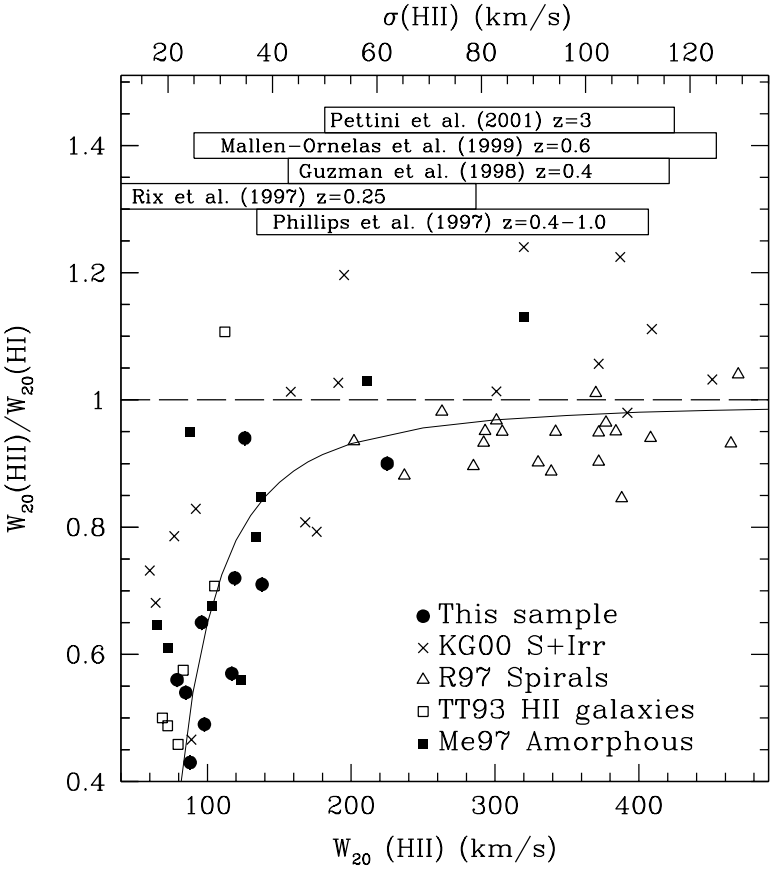

Fig. 5.— Comparison of the observed H II linewidths (i.e., not corrected for inclination) versus the ratio of H II-to-H I linewidths. Filled circles denote our sample, crosses denote the sample of spiral & irregular galaxies studied by Kobulnicky & Gebhardt (2000), open triangles denote the spiral sample of Raychaudhury et al. (1997), and open squares are the H II galaxies from Telles & Terlevich (1993) with H I widths as measured by Smoker et al. (2000). The measured H II-to-H I ratio departs systematically from unity for galaxies with small H II linewidths. The solid line is an approximate fit to the data: $W_{\rm H\ II}/W_{\rm H\ I} = 1 - 5W_{\rm H\ II}^{-1} - 500W_{\rm H\ II}^{-2} - 2.5 \times 10^5 W_{\rm H\ II}^{-3}$ The boxes at the top of the figure illustrate the range of velocity widths measured for compact galaxies in the Hubble Deep Field flanking fields (Phillips et al. 1997), $z \sim 0.6$ field galaxies (Mallén-Ornelas et al. 1999), $z \sim 0.25$ field galaxies (Rix et al. 1997), and compact blue galaxies at $z \sim 0.4$ (Guzmán et al. (1998). Our sample of compact blue galaxies have $W_{\rm H\ II}/W_{\rm H\ I} \sim 0.6$ similar to the ratio for H II galaxies studied by Telles & Terlevich (1993). This effect is capable of reducing the T-F offsets found at intermediate redshifts by some studies.

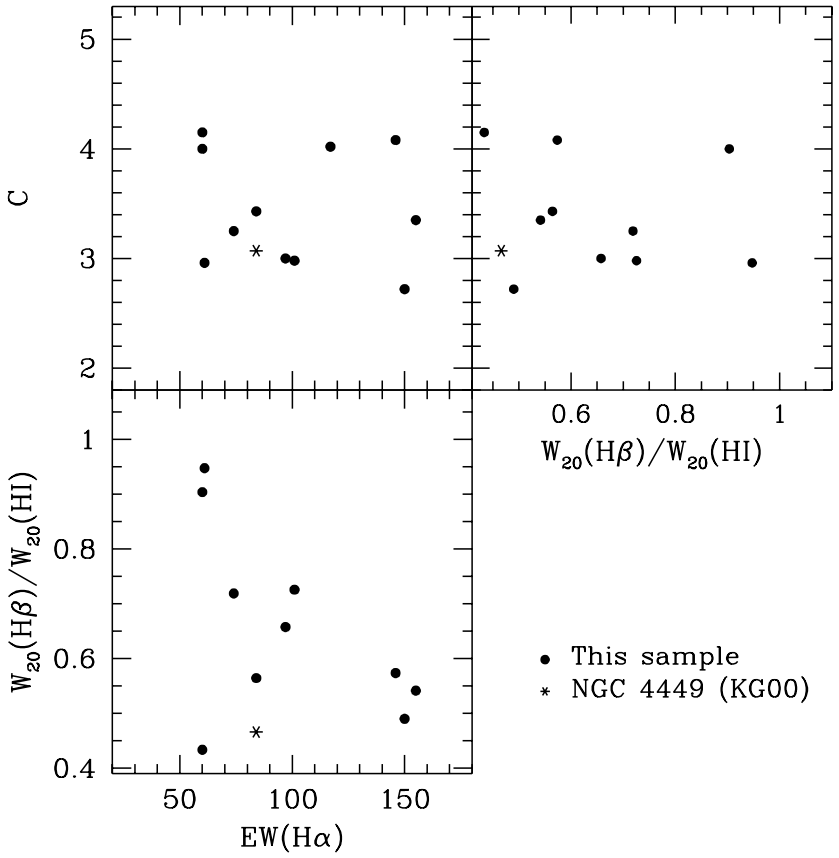

Fig. 6.— Diagnostic parameters of the nearby galaxy sample (filled circles), illustrating the relation between linewidth ratio, (W_{20}(H II)/W_{20}(H I)), Hα equivalent width, $EW(H\alpha)$, and concentration index, C. The nearby irregular galaxy NGC 4449, marked by a star, is included as a comparison object. Objects with high $EW(H\alpha)$ tend to have the smallest H II/HI linewidths, although the dispersion is large.

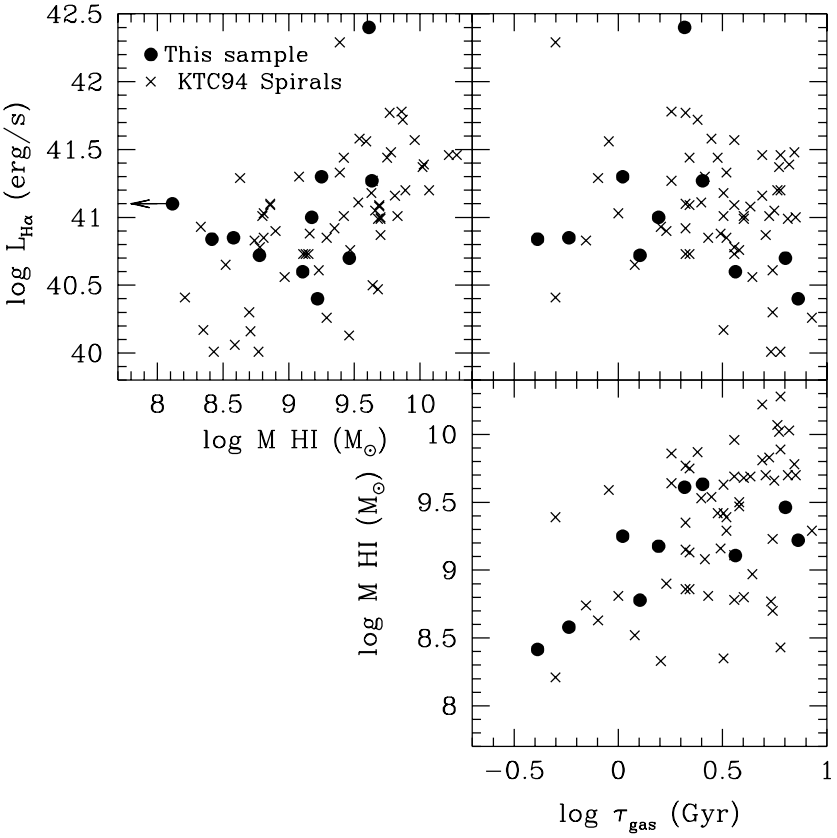

Fig. 7.— A comparison of $M_{H\ I}$ and $L_{H\alpha}$ (upper left panel), τ_{gas} and $L_{H\alpha}$ (upper right panel), and $M_{H\ I}$ and τ_{gas} (lower right panel) for the UCM BCG analogs (filled circles) and a sample of spiral galaxies from Kennicutt *et al.* (1994; crosses). It is evident that the two samples of galaxies occupy a similar region of parameter space in all three plots, although a couple of UCM galaxies do have much shorter τ_{gas} than the Kennicutt *et al.* (1994) sample. The upper limit of $M_{H\ I}$ and τ_{gas} for UCM 2351+2321 is off the left side of the plot.

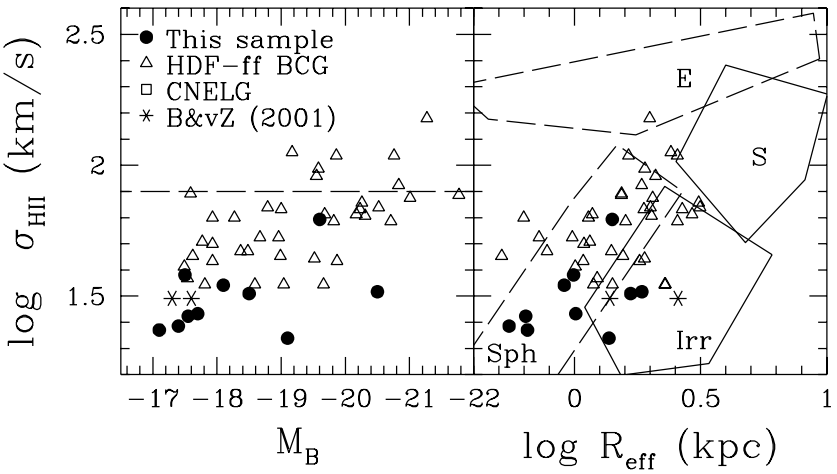

Fig. 8.— A comparison of the sample galaxies (filled circles) with the same intermediate-redshift BCGs (squares and triangles) from Figure 1. The left panel compares the velocity dispersion with absolute blue magnitude (M_B). The right panel compares the emission line velocity dispersion, $\sigma_{\rm H\ II}$, (not corrected for inclination) with the logarithm of the effective radius (R_{eff}). The velocity dispersion is measured via the Hβ line for our sample, and via a combination of Hβ, [O II], and [O III] linewidths for the intermediate redshift BCGs. Our sample galaxies have smaller velocity dispersions than the intermediate redshift BCGs, on average.

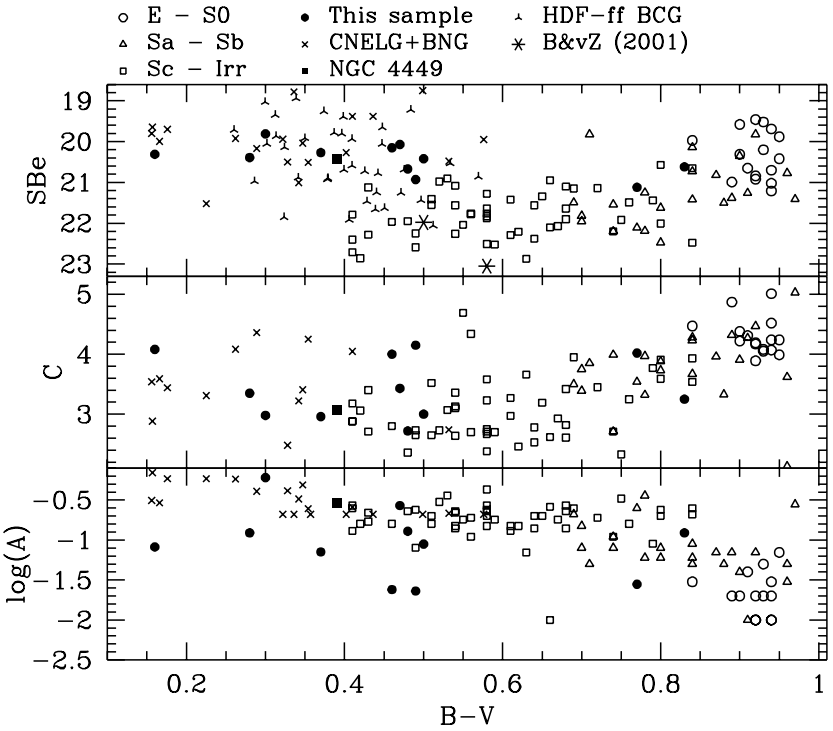

Fig. 9.— Diagnostic parameters including color (B-V), B-band surface brightness (SBe in mag $arcsec^{-2}$), concentration index (C), and asymmetry (A). Filled circles denote our sample, open symbols denote nearby galaxies from the Frei (1999) catalog taken from Bershady et al. (2000). Crosses and upside-down 'Y's denote the BCG collection of Jangren et al. (2000). Note that our sample of nearby compact galaxies shares a unique space in these diagrams with the intermediate-redshift BCGs, indicating that analogs of the intermediate-redshift compact galaxies can be found among our sample.

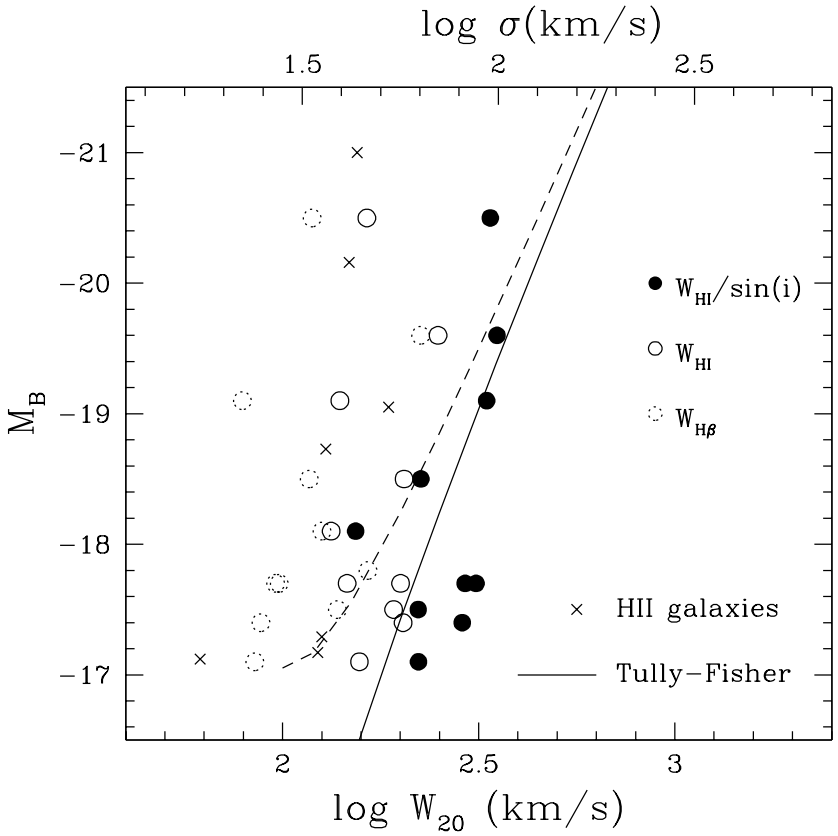

Fig. 10.— Comparison between our sample galaxy kinematics (circles), H II galaxies (crosses) from Telles & Terlevich (1993) and the canonical Tully-Fisher relation (solid line: $M_B = -6.86 \log(W_R) - 2.27$ from Pierce & Tully 1988). The raw H II velocity widths (dashed circles) for our sample are most consistent with the locus of the H II galaxies. The H I velocity widths (open circles) are closer to the Tully-Fisher relation. But the inclination-corrected H I velocity widths (filled circles) are consistent with the Tully-Fisher without any luminosity offsets. The dashed curve shows how the T-F relation would be modified if measured using inclination-corrected optical line-widths, based on the relation adopted in Fig. 5.